

1        **Secondary formation of nitrated phenols: insights from observations**  
2                    **during the Uintah Basin Winter Ozone Study (UBWOS) 2014**

3    Bin Yuan<sup>1,2</sup>, John Liggio<sup>3</sup>, Jeremy Wentzell<sup>3</sup>, Shao-Meng Li<sup>3</sup>, Harald Stark<sup>2,4</sup>, James M.  
4    Roberts<sup>1</sup>, Jessica Gilman<sup>1,2</sup>, Brian Lerner<sup>1,2</sup>, Carsten Warneke<sup>1,2</sup>, Rui Li<sup>1,2</sup>, Amy  
5    Leithead<sup>3</sup>, Hans D. Osthoff<sup>5</sup>, Robert Wild<sup>1,2</sup>, Steven S. Brown<sup>1,6</sup>, and Joost A. de  
6    Gouw<sup>1,2,6</sup>

7    1. NOAA Earth System Research Laboratory (ESRL), Chemical Sciences Division,  
8    Boulder, CO, USA

9    2. Cooperative Institute for Research in Environmental Sciences, University of Colorado  
10   at Boulder, Boulder, CO, USA

11   3. Environment Canada, Science and Technology Branch, Toronto, ON, Canada

12   4. Aerodyne Research Inc., Billerica, MA, USA

13   5. Department of Chemistry, University of Calgary, Calgary, Canada

14   6. Department of Chemistry and Biochemistry, University of Colorado at Boulder, CO,  
15   USA

16

17

18 **Abstract**

19 We describe the results from online measurements of nitrated phenols using a time  
20 of flight chemical ionization mass spectrometer (ToF-CIMS) with acetate as reagent ion  
21 in an oil and gas production region in January and February of 2014. Strong diurnal  
22 profiles were observed for nitrated phenols, with concentration maxima at night. Based  
23 on known markers ( $\text{CH}_4$ ,  $\text{NO}_x$ ,  $\text{CO}_2$ ), primary emissions of nitrated phenols were not  
24 important in this study. A box model was used to simulate secondary formation of  
25 phenol, nitrophenol (NP) and dinitrophenols (DNP). The box model results indicate that  
26 oxidation of aromatics in the gas phase can explain the observed concentrations of NP  
27 and DNP in this study. Photolysis was the most efficient loss pathway for NP in the gas  
28 phase. We show that aqueous-phase reactions and heterogeneous reactions were minor  
29 sources of nitrated phenols in our study. This study demonstrates that the emergence of  
30 new ToF-CIMS (including PTR-TOF) techniques allows for the measurement of  
31 intermediate oxygenates at low levels and these measurements improve our  
32 understanding on the evolution of primary VOCs in the atmosphere.

33

## 34 1. Introduction

35 Nitrated phenols are a family of aromatic compounds with both nitro (-NO<sub>2</sub>) and  
36 hydroxyl groups (-OH) connected to a benzene ring. Nitrated phenols have been detected  
37 in the gas phase, aerosol, cloud water and rainwater (Harrison et al., 2005a). Many  
38 studies have shown that nitrated phenols are one of the important components of brown  
39 carbon in aerosol (Desyaterik et al., 2013; Mohr et al., 2013; Zhang et al., 2013; Lin et al.,  
40 2015), as they absorb light in the atmosphere (Bejan et al., 2007). Photolysis of some  
41 nitrated phenols was reported to produce nitrous acid (HONO) (Bejan et al., 2006) and  
42 hydroxyl (OH) radicals (Cheng et al., 2009), while the oxidation and photolysis of them  
43 contribute to secondary organic aerosol (SOA) formation, especially in biomass burning  
44 plumes (Mohr et al., 2013; Kitanovski et al., 2012; Lauraguais et al., 2014). There is also  
45 evidence that nitrated phenols are phytotoxic and contribute to forest decline (Rippen et  
46 al., 1987; Natangelo et al., 1999). Some nitrated phenols are known to be mutagenic and  
47 are of concern to human health (Fernandez et al., 1992).

48 Sources of nitrated phenols in the atmosphere include emissions from vehicle  
49 exhaust (Inomata et al., 2013; Tremp et al., 1993; Sekimoto et al., 2013) and biomass  
50 burning (Mohr et al., 2013). Nitrated phenols are also produced from photooxidation of  
51 aromatic hydrocarbons in the atmosphere: for example benzene oxidizes to 2-nitrophenol  
52 (2-NP) and 4-nitrophenol (4-NP), and toluene oxidizes to methylnitrophenols (MNP)  
53 (Harrison et al., 2005a). Figure 1 shows the reactions leading to secondary formation of  
54 NP and dinitrophenols (DNP) in the atmosphere (Jenkin et al., 2003). Oxidation of  
55 benzene by OH radicals forms phenol and further reactions of phenol with either OH or  
56 NO<sub>3</sub> radicals yield phenoxy (C<sub>6</sub>H<sub>5</sub>O) radicals, which react further with NO<sub>2</sub> to generate  
57 NP. In addition to benzene oxidation, C<sub>6</sub>H<sub>5</sub>O radicals are also generated from the reaction  
58 of NO with phenyl peroxy (C<sub>6</sub>H<sub>5</sub>O<sub>2</sub>) radicals, a product from reactions of some other  
59 aromatic precursors, e.g. benzaldehyde (Caralp et al., 1999). Further oxidation of nitrated  
60 phenols by obtaining another nitro- group produces dinitrophenols (DNP). The yields of  
61 NP from phenol oxidation by OH radicals (Atkinson et al., 1992; Olariu et al.,  
62 2002; Berndt and Boge, 2003) and NO<sub>3</sub> radicals (Atkinson et al., 1992; Bolzacchini et al.,  
63 2001) have been reported. Berndt and Boge (2003) also showed that the NP yield from

64 OH oxidation of phenol increases at higher NO<sub>2</sub> concentrations. In addition to gas phase  
65 reactions, nitrated phenols are formed from aqueous-phase reactions in aerosol or cloud  
66 water (Vione et al., 2001, 2005). The importance of the aqueous reactions compared to  
67 gas-phase reactions is highly dependent on liquid water content in the atmosphere  
68 (Harrison et al., 2005b).

69 The sinks of nitrated phenols in the gas phase include reactions with OH radicals  
70 (Atkinson et al., 1992;Bejan et al., 2007), with NO<sub>3</sub> radicals (Atkinson et al., 1992), with  
71 chlorine atoms (Bejan et al., 2015) and photolysis (Bejan et al., 2007;Chen et al., 2011).  
72 It has been proposed that photolysis is the dominant gas phase atmospheric loss for  
73 nitrated phenols (Bejan et al., 2007). Despite the importance of photolysis of nitrated  
74 phenols, the photolysis frequency of nitrated phenols under ambient conditions was only  
75 reported in a single non-peer reviewed publication (1.4% of photolysis frequency of NO<sub>2</sub>)  
76 (Bardini, 2006). The chemical products from photolysis of nitrated phenols were  
77 proposed, but the proposed products were not fully evaluated against experimental results  
78 (Bejan et al., 2006). Nitrated phenols are also removed by various processes in the  
79 aqueous phase, including reactions with OH, NO<sub>3</sub> and photolysis (Vione et al., 2009).

80 Measurements of nitrated phenols have been mainly conducted using offline  
81 methods (Harrison et al., 2005a). Air samples are usually collected on filters or cartridges  
82 and then analyzed by liquid chromatography (LC) methods (Rubio et al., 2012;Harrison  
83 et al., 2005a;Delhomme et al., 2010). These detection methods are time-consuming and  
84 measurements as a function of the time of day are not usually possible (Delhomme et al.,  
85 2010). The lack of fast-response online measurements has prevented, at least partially, a  
86 thorough investigation of sources and sinks of nitrated phenols. Recently, Mohr et al.  
87 (2013) deployed a chemical ionization mass spectrometer (CIMS) using acetate as the  
88 reagent ion to measure nitrated phenols online in the particle phase in winter of London  
89 and based on their measurements the authors concluded that nitrated phenols were mainly  
90 from wood burning in this region of the atmosphere.

91 In this study, we conducted high time resolution measurements of nitrated phenols  
92 in the gas phase at a site in an oil and gas production region in winter. High  
93 concentrations of ozone and secondary products (Edwards et al., 2014) were observed at

94 this site, as the result of photochemical degradation of large amounts of alkanes and  
95 aromatics emitted from oil and gas production in this region (Warneke et al., 2014).  
96 Using the present dataset, we investigate diurnal variations, sources and sinks of nitrated  
97 phenols. We use a box model to analyze the budget of nitrated phenols in the atmosphere,  
98 and provide insights into the formation mechanism of nitrated phenols.

## 99 **2. Measurements**

100 The Uintah Basin Winter Ozone Study (UBWOS 2014) was conducted in January  
101 and February of 2014 at the Horse Pool site in the Uintah Basin, where over 10,000  
102 active oil and gas wells are located.

### 103 **2.1 Acetate ToF-CIMS**

#### 104 2.1.1 Instrument operation

105 An Aerodyne time-of-flight (ToF) CIMS (Lee et al., 2014) that uses acetate  
106 ( $\text{CH}_3\text{C}(\text{O})\text{O}^-$ ) as the reagent ion was deployed at the Horse Pool site during the UBWOS  
107 2014 to measure organic acids, inorganic acids and nitrated phenols. These compounds  
108 are ionized in the ion-molecule reaction region (IMR,  $61.8 \pm 0.3$  mbar) via proton  
109 abstraction (Veres et al., 2008) or by a sequence of clustering-declustering/deprotonation  
110 reactions (Brophy and Farmer, 2015) in the reaction with acetate ions. Acetate ions were  
111 produced by introducing saturated acetic anhydride/ $\text{N}_2$  mixture (5 mL/min) mixed with  
112 another flow of  $\text{N}_2$  (2.5 L/min) into a polonium-210 ( $^{210}\text{Po}$ ) radioactive source. The  
113 instrument was operated at strong de-clustering conditions by applying voltages in the  
114 first quadrupole ion guide (i.e. SSQ,  $2.50 \pm 0.01$  mbar) during UBWOS 2014, with the  
115 ratio of acetate cluster ( $\text{CH}_3\text{C}(\text{O})\text{O}^- \cdot \text{CH}_3\text{C}(\text{O})\text{OH}$ )/acetate ( $\text{CH}_3\text{C}(\text{O})\text{O}^-$ ) at  $0.4\% \pm 0.1\%$ .  
116 Under such de-clustering conditions, the conjugate anions were usually observed as the  
117 product ions, with little contribution from cluster ions. The reagent ions and product ions  
118 are analyzed using a high-resolution time of flight mass spectrometer (Tofwerk AG,  
119 Switzerland). The signals of acetate ion were approximately  $1\text{-}2 \times 10^6$  count per second  
120 (cps) during the campaign (ToF extraction frequency=25 kHz). The mass resolution of  
121 the ToF analyzer during UBWOS 2014 was approximately 3200 for ions of  $m/z > 200$ .

122 Background signals associated with the instrument were measured every 2 hours  
123 for 15 min by passing ambient air through three stages of zero air generation: a platinum  
124 catalytic converter heated to 350 °C, nylon wool coated with sodium bicarbonate  
125 (NaHCO<sub>3</sub>), and activated charcoal, which were used in series to remove acidic gases  
126 from the sample air and determine instrument backgrounds. During the UBWOS 2014  
127 study, two CIMS inlets constructed from Teflon tubing heated to ~40 °C with similar  
128 lengths (~10 m) placed at heights of 1 m and 18.5 m above ground were switched  
129 automatically every 30 min during the period of January 24- February 1, to measure the  
130 vertical concentration gradient of nitrated phenols and other acidic gases. Inlet switching  
131 between a long-heated and a short-unheated inlet was conducted during February 1-5, to  
132 explore possible inlet interferences to CIMS measurements of nitrated phenols from the  
133 long-heated inlet. We did not observe differences in signals between the long and short  
134 inlets for nitrated phenols except DNP (Figure S1), indicating that potential loss in the  
135 sampling line was minimal for the reported single nitrated phenols in this study. The inlet  
136 issues for DNP will be discussed in Section 2.1.2.

### 137 2.1.2 Data processing

138 The ToF-CIMS data was processed using the Tofware software package  
139 ([www.tofwerk.com/tofware](http://www.tofwerk.com/tofware)) written in Igor Pro (Wavemetrics Inc., USA). The detailed  
140 data processing procedures are presented in recent studies (Yatavelli et al., 2014; Stark et  
141 al., 2015). Post-measurement mass calibrations were performed using nine isolated ions,  
142 including  $m/z$  31.9904 (O<sub>2</sub><sup>-</sup>),  $m/z$  34.9694 (Cl<sup>-</sup>),  $m/z$  44.9982 (CHO<sub>2</sub><sup>-</sup>),  $m/z$  59.0139  
143 (C<sub>2</sub>H<sub>3</sub>O<sub>2</sub><sup>-</sup>),  $m/z$  61.9884 (NO<sub>3</sub><sup>-</sup>),  $m/z$  143.9840 (C<sub>3</sub>F<sub>4</sub>O<sub>2</sub><sup>-</sup>),  $m/z$  162.9824 (C<sub>3</sub>F<sub>5</sub>O<sub>2</sub><sup>-</sup>),  $m/z$   
144 193.9808 (C<sub>4</sub>F<sub>6</sub>O<sub>2</sub><sup>-</sup>) and  $m/z$  243.9776 (C<sub>3</sub>F<sub>8</sub>O<sub>2</sub><sup>-</sup>). The four fluorine-containing ions in the  
145 list were released from the Teflon inlet during UBWOS 2014 and their persistent  
146 presence was used for mass calibration. The accuracy of mass calibration was 4.7±1.9  
147 ppm for the whole campaign and the errors of mass calibration for individual ions were  
148 usually within 10 ppm (average+3σ). The fitted raw signals for the targeted compounds  
149 were normalized using an acetate signal at the level of 1×10<sup>6</sup> cps.

150 The fitted  $m/z$  used for quantification of concentrations of nitrated phenols in the  
151 acetate CIMS are  $m/z$  138.0197 (C<sub>6</sub>H<sub>4</sub>NO<sub>3</sub><sup>-</sup>) for NP,  $m/z$  152.0353 (C<sub>7</sub>H<sub>6</sub>NO<sub>3</sub><sup>-</sup>) for MNP,

152  $m/z$  166.0510 ( $C_8H_8NO_3^-$ ) for dimethylnitrophenol+ ethylnitrophenol (DMNP) and  $m/z$   
153 183.0047 ( $C_6H_3N_2O_5^-$ ) for DNP. Compounds with the same molecular formulas as  
154 nitrated phenols include phenyl nitrates/benzyl nitrates, methoxynitrobenzenes,  
155 nitrobenzyl alcohols and hydroxycarboxylic acids derived from pyridine. The first three  
156 groups of compounds have lower acidities than acetic acid (Bartmess, 2015) and hence  
157 they are unlikely to be observed in acetate CIMS, while hydroxycarboxylic acids derived  
158 from pyridine are expected to be small in the atmosphere.

159 High-resolution (HR) peak fitting to  $m/z$  138,  $m/z$  152 and  $m/z$  183 in the averaged  
160 mass spectra of ToF-CIMS on a typical day (January 25, 2014) are shown as examples in  
161 Figure 2. Isotope signals from lower masses (dark green lines) accounted for small  
162 fractions of the  $m/z$  signals. Multiple overlapping ion peaks were identified in the  $m/z$   
163 channels. In addition to nitrated phenols, several ions without deprotonation were also  
164 present in the even  $m/z$  (e.g.  $C_8H_{10}O_2^-$  at  $m/z$  138), possibly due to electron transfer  
165 reactions and/or fragmentation in the quadrupole ion guides (Stark et al., 2015). The  
166 signals of NP and MNP were either the largest or significantly larger than their  
167 neighboring peaks at their respective  $m/z$ , whereas the signal of DNP was much smaller  
168 than its neighboring peaks on January 25, 2014. Smaller ratios of the signals between the  
169 targeted peak and its neighboring peaks have been shown to deteriorate the precision of  
170 the fitted signals for the targeted peak (Cubison and Jimenez, 2015; Müller et al.,  
171 2011; Corbin et al., 2015). Based on the provided equations in Cubison and Jimenez  
172 (2015), the imprecision arising from mass calibration (not including counting error) for  
173 the signals of NP, MNP and DNP are 3.2%, 1.8% and 47% based on the mass spectra of  
174 January 25, respectively. Imperfect mass calibration can also affect fitted magnitudes of  
175 ion signals. Figure S2 shows the sensitivity of the fitted signals of various masses as a  
176 function of the errors in mass calibration. The signal changes at 10 ppm (average+3 $\sigma$ )  
177 error of mass calibration relative to the perfect mass calibration (error=0 ppm) for NP,  
178 MNP and DNP signals are as high as 14%, 5% and 81%, respectively. The results from  
179 both precision calculation and sensitivity of fitted magnitudes indicate that the peak  
180 signals of NP and MNP can be fitted well with low uncertainties. The peak fitting at  $m/z$   
181 166 for DMNP shows similar results as  $m/z$  138 for NP and  $m/z$  152 for MNP. However,  
182 large uncertainties are associated with the peak signals of DNP on January 25, 2014,

183 which is mainly affected by the  $\text{C}_3\text{F}_6\text{HO}_2^-$  ions ( $m/z$  182.9886) as indicated by the  
184 opposite behaviors of the DNP ion and  $\text{C}_3\text{F}_6\text{HO}_2^-$  ion in Figure S2C.

185 The  $\text{C}_3\text{F}_6\text{HO}_2^-$  ion ( $m/z$  182.9886) was released from the heated Teflon inlet along  
186 with other fluorine-containing ions that were used for mass calibration. The release of  
187  $\text{C}_3\text{F}_6\text{HO}_2^-$  ion was supported by much higher signals from the long-heated inlet compared  
188 to the short-unheated inlet, when inlet-switching experiments were conducted in February  
189 2-5 (Figure S1). Long-heated inlets were used for most of the time during UBWOS 2014  
190 (January 23- February 13), except during January 18-22, when a short-unheated inlet was  
191 used. The averaged mass spectra of  $m/z$  183 measured on January 18 is shown in Figure  
192 2D. Compared to the mass spectra on January 25,  $\text{C}_3\text{F}_6\text{HO}_2^-$  signals on January 18 were  
193 lower and the signals of DNP were larger than of  $\text{C}_3\text{F}_6\text{HO}_2^-$  ions. As a result, the  
194 uncertainty from peak fitting for the DNP ion was much lower on January 18 (Figure  
195 S2D). Thus, we will only use measured DNP data in the beginning of the campaign  
196 (January 18-22), when the long heated inlet was not connected to the acetate CIMS and  
197 no inlet switching was performed.

198 The response of the CIMS instrument for nitrated phenols, including 2-NP, 4-NP, 2-  
199 methyl-4-nitrophenol and 2,5-dinitrophenol, was calibrated using a Liquid Calibration  
200 Unit (LCU, IONICON Analytik). In the LCU, a water solution with known  
201 concentrations of the targeted compounds is nebulized and diluted by another gas stream  
202 at different flow rates to produce a gas standard at various concentrations (Kaser et al.,  
203 2013). The results of the calibrations to various nitrated phenols are shown in Table 1.  
204 The sensitivity of 4-NP in our instrument was determined to be higher than that of 2-NP  
205 by a factor of 2.1. A higher sensitivity of 4-NP in acetate CIMS was reported in Mohr et  
206 al. (2013), but in that study the difference was significantly larger at three orders of  
207 magnitude (Mohr et al., 2013). The different sensitivity ratios of 4-NP/2-NP can be  
208 caused by many different instrumental conditions between our instrument and that in  
209 Mohr et al. (2013), such as the amount of acetic anhydride introduced into the instrument,  
210 IMR and SSQ pressures, and de-clustering settings in the quadrupole ion guides, all of  
211 which affect sensitivities of acetate CIMS significantly (Stark et al., 2012). The main  
212 reagent ions in IMR were shown to be acetic acid-acetate clusters rather than acetate  
213 (Bertram et al., 2011) and the cluster distributions in IMR may depend on operated

214 pressure in IMR and the amount of acetic anhydride introduced into the ion source. While  
215 de-clustering in SSQ helps the interpretation of recorded mass spectra, de-clustering also  
216 obscures a precise understanding of cluster distributions in IMR and hence accurate  
217 prediction of sensitivities in acetate CIMS. This result also emphasizes the importance of  
218 instrument calibrations in deriving concentration from acetate CIMS. We note that 3-  
219 nitrophenol (3-NP) is not usually present in the atmosphere (Harrison et al., 2005a).  
220 Thus, the average of the sensitivities of 2-NP and 4-NP was used for calculating  
221 concentrations of NP. DMNP was not calibrated in this study and we assumed the same  
222 sensitivity as determined for MNP.

223 The accuracies of nitrated phenols measurements by the CIMS are conservatively  
224 estimated to be around 40% for NP and 50% for other nitrated phenols, mainly arising  
225 from uncertainties in the concentration output of the LCU (~10%), uncertainties  
226 associated with calibration procedures (~5%), errors in high-resolution (HR) peak fittings  
227 to mass spectra (see above and Figure S2), and the representativeness of the calibrated  
228 species to other isomers (0-30% for NP and 0-40% for other nitrated phenols). Assuming  
229 random errors in the observed ion counts follow a Poisson distribution, detection limits of  
230 nitrated phenols, i.e. concentrations with a signal to noise ratio (S/N) of 3, are calculated  
231 to be 0.1-0.3 ppt for 1-min average data (Table 1). Following the discussions in Bertram  
232 et al. (2011), the measured background ion counts in ToF-CIMS drift over time and thus  
233 detection limits are more appropriately calculated as the concentrations at three times the  
234 standard deviation of the measurement background counts. The determined detection  
235 limits of nitrated phenols increase to the range of 0.3-0.5 ppt based on this approach  
236 (Bertram et al., 2011) (Table 1).

## 237 **2.2 Other measurements**

238 Volatile organic compounds (VOCs), including hydrocarbons and oxygenates, were  
239 measured using an online gas chromatograph-mass spectrometer (GC-MS) (Gilman et al.,  
240 2013). A commercial proton transfer reaction time of flight mass spectrometer (PTR-  
241 TOF) (IONICON Analytik, Austria) was also deployed at the Horse Pool site to measure  
242 various VOC species (Warneke et al., 2015). Measurements of phenol, cresols and  
243 dimethylphenols+ethylphenols (DMP) were accomplished by the PTR-TOF at  $m/z$

244 95.0491 ( $C_6H_6OH^+$ ),  $m/z$  109.0648 ( $C_7H_8OH^+$ ) and  $m/z$  123.0804 ( $C_8H_{10}OH^+$ ),  
245 respectively. An example of high-resolution peak fitting to  $m/z$  95 in the mass spectra of  
246 the PTR-TOF is shown in Figure S3. The sensitivities to these phenols are estimated here  
247 from the calibrated sensitivities of  $m/z$  93.0699 (toluene),  $m/z$  107.0855 (C8-aromatics)  
248 and  $m/z$  121.1012 (C9-aromatics) and the ratio of proton-transfer rate coefficients ( $k$ ) of  
249 the phenols versus the aromatic hydrocarbons (Cappellin et al., 2012) (see details in the  
250 SI). Considering the uncertainties in the rate coefficients  $k$ , the accuracies of the  
251 determined concentrations of phenols can be up to 50% (de Gouw and Warneke, 2007).

252 Measurements of  $NO_3$  and  $N_2O_5$  were conducted by a cavity ring-down  
253 spectroscopy instrument (Dubé et al., 2006).  $NO_x$  ( $NO+NO_2$ ),  $NO_y$  and  $O_3$  were  
254 measured with another cavity ring-down spectroscopy instrument (Wild et al., 2014).  
255 Measurements of methane ( $CH_4$ ) and carbon dioxide ( $CO_2$ ) were performed with a  
256 commercial cavity ring-down spectrometry instrument (Picarro G2301). A pair of  
257 commercial spectral radiometers (Metcon Inc.) was used to measure photolysis  
258 frequencies of ozone and  $NO_2$ .

### 259 **3. Results and Discussions**

#### 260 **3.1 Diurnal variations**

261 Measured diurnal profiles of NP, MNP and DMNP during the UBWOS 2014 are  
262 shown in Figure 3. Very strong diurnal variations in concentrations of these nitrated  
263 phenols were observed. Concentrations of nitrated phenols were higher at night and lower  
264 in the daytime. The ratios between the concentrations in the two hours around midnight  
265 (23:00-1:00 MST) and in the two hours around noon (11:00-13:00 MST) are 2.9, 3.9 and  
266 4.7 for NP, MNP and DMNP, respectively. This indicates that the substituted alkyl  
267 groups enhance the diurnal variations of nitrated phenols, either through larger source at  
268 night or stronger loss in the daytime.

269 Primary emissions of VOCs and  $NO_x$  at the Horse Pool site are predominantly due  
270 to oil and gas production activities, as the Horse Pool site is surrounded by oil and gas  
271 production wells. VOCs and  $NO_x$  emitted from nearby oil and gas wells led to periodic  
272 concentration spikes during the UBWOS campaigns (Warneke et al., 2014; Yuan et al.,  
273 2015). Figure 4 shows two types of episodes encountered during UBWOS 2014. The first

274 was associated with high concentrations of methane and benzene, as an example of  
275 fugitive emissions from oil and gas wells. No enhancement of nitrated phenols was  
276 observed for the first emission episode. The second episode was associated with high  
277 concentrations of  $\text{NO}_y$ ,  $\text{NO}_x$  and  $\text{CO}_2$ , as an example of either vehicular emissions or  
278 other fuel combustion activities related to oil and gas extractions (e.g., compressors,  
279 dehydrators and pump jacks). High  $\text{NO}_x/\text{NO}_y$  ratios ( $0.96 \pm 0.01$ ) indicate that a fresh  
280 combustion plume was encountered. We observed small enhancement of NP during the  
281 second emission episode. The enhancement ratio of NP/ $\text{NO}_y$  in this plume is determined  
282 to be  $4.6 \pm 0.7 \times 10^{-3}$  ppt/ppb, which is comparable with the reported NP/ $\text{NO}_x$  emission  
283 ratios ( $1-50 \times 10^{-3}$  ppt/ppb) from gasoline and diesel vehicles (Inomata et al.,  
284 2013; Sekimoto et al., 2013). Using the obtained enhancement ratio of NP/ $\text{NO}_y$ , we  
285 determine that primary emissions from combustion sources only account for less than 2%  
286 of NP concentrations during UBWOS 2014. In addition to these primary sources,  
287 biomass burning was not observed in the UBWOS campaigns, based on the absence of  
288 any enhancement of biomass burning markers like acetonitrile. We conclude that primary  
289 emissions of nitrated phenols were not significant during UBWOS 2014.

290 In addition to primary emissions, secondary formation from oxidation of phenols is  
291 an important source for nitrated phenols (Harrison et al., 2005a). Phenol exhibited a  
292 concentration maximum in the afternoon (Figure 3B). The diurnal profile of phenol is  
293 more similar to that of secondary acetaldehyde, than that of primary emitted benzene. It  
294 suggests that secondary formation was the most important source of phenol. Substituted  
295 phenols (cresols and DMP) also had similar diurnal variations as phenol.

## 296 **3.2 Modeling analysis for NP**

### 297 3.2.1 Box model results

298 We will focus on NP to understand the budget of nitrated phenols, because NP had  
299 higher concentrations than the substituted nitrated phenols (MNP and DMNP) and there  
300 is more information on sources and sinks of NP in the literature. A series of zero-  
301 dimensional box model simulations on the formation of phenol and NP were conducted  
302 using the online AtChem tool (<https://atchem.leeds.ac.uk>). The MCM v3.2 (Jenkin et al.,  
303 2012) was used as the chemical mechanism in the box model. We note that ambient

304 temperature ( $-5\pm 5$  °C) during UBWOS 2014 was much lower than the temperature  
305 (around 25 °C) at which rate constants of many reactions are usually measured. Rate  
306 constants as a function of temperature are only available for the reactions of OH radical  
307 with benzene and phenol among those shown in Figure 1 and they were already included  
308 in the MCM v3.2. The model ran in a time-dependent mode and a 48-hour spin-up time  
309 was applied in the box model. Measured concentrations of various hydrocarbons, NO<sub>x</sub>,  
310 O<sub>3</sub>, NO<sub>3</sub> and photolysis frequencies (Table S2) were used as constraints in the box model.  
311 The simulation period of the model was chosen to be January 18-27, a period associated  
312 with several buildup episodes of ozone and other secondary products, with high measured  
313 concentrations of NP and without precipitation. Following previous box model studies  
314 (Yuan et al., 2015; Edwards et al., 2014), dilution and deposition processes were  
315 represented together using a diurnally varying first-order physical loss parameter in the  
316 box model. The physical loss rate at night ( $5.8\times 10^{-6}$  s<sup>-1</sup>) was calculated from the decrease  
317 rate of NP concentration between 0:00-6:00 am when the chemical loss was expected to  
318 be low (see Section 3.3.4). A higher physical loss rate ( $2.0\times 10^{-5}$  s<sup>-1</sup>) during daytime was  
319 used to account for larger turbulent mixing during daytime (Edwards et al., 2014), which  
320 results in the decrease of concentrations of inert tracers in the afternoon, e.g. benzene  
321 (Figure 3) and methane. Based on sensitivity tests of the box model, increase and  
322 decrease of the physical loss rate terms by a factor of two resulted in -48% and +39% of  
323 changes in the modeled NP concentrations.

324 As shown in the introduction section, photolysis has been recognized as an  
325 important sink for nitrated phenols. However, the photolysis of NP (and other nitrated  
326 phenols) is not included in the MCM v3.2. We added the photolysis frequency of NP  
327 from Bardini (2006) (1.4% of photolysis frequency of NO<sub>2</sub>) into the MCM v3.2 and this  
328 model run is referred to as the base simulation. Here, we assume that photolysis of NP  
329 produces 2-phenoxy biradicals and HONO, as proposed in Bejan et al. (2006) (Figure 1  
330 Route1). There are other possible chemical routes for photolysis of NP: producing  
331 phenoxy radicals (C<sub>6</sub>H<sub>5</sub>O) by losing NO<sub>2</sub> (Route2 in Figure 1) and producing  
332 nitrophenoxy radical by hydrogen abstraction (Route3 in Figure 1). The simulation test in  
333 Figure S4 indicates that the pathway forming C<sub>6</sub>H<sub>5</sub>O radicals and NO<sub>2</sub> is an ineffective  
334 sink for NP, since C<sub>6</sub>H<sub>5</sub>O radical will re-form NP by reacting with NO<sub>2</sub>. However, we

335 cannot exclude this pathway to occur along with that producing 2-phenoxy biradicals and  
336 HONO. The photolysis frequency determined in Bardini (2006) based on concentration  
337 changes of 2-nitrophenol in a chamber may not include this pathway as well. As a result,  
338 attributing the photolysis rates determined in Bardini (2006) to other pathways other than  
339 Route2 is reasonable. The route producing nitrophenoxy radical will be discussed in  
340 Section 3.3.

341 The simulated results for phenol and NP from the base case of the box model are  
342 shown in Figure 5. The modeled diurnal variations agreed reasonably well with the  
343 observation for both NP and phenol in the base simulation, except for the phenol  
344 nighttime levels that will be discussed below. Although modeled NP concentrations are  
345 higher than the measurements for both daytime and nighttime, the agreement between  
346 measurements and model results is still within their combined uncertainties.

347 The average measured concentrations of phenol at night are higher than 10 ppt, but  
348 the modeled phenol concentrations are usually less than 2 ppt. At night, the production of  
349 phenol from benzene oxidation halts, and the fast reaction with  $\text{NO}_3$  ( $2.8 \times 10^{-11} \text{ cm}^3$   
350  $\text{molecule}^{-1} \text{ s}^{-1}$  at 298 K) removes phenol quickly (Figure 7 and discussion in Section  
351 3.2.3). Measured nighttime  $\text{NO}_3$  radicals were quite low during UBWOS 2014 ( $1.4 \pm 2.4$   
352 ppt). As a check on the possible uncertainties in measurements of  $\text{NO}_3$  at these low  
353 levels, simulations by varying  $\text{NO}_3$  concentrations by a factor of 2 result in little  
354 improvement for the modeled concentrations of phenol (Figure S5). Another simulation  
355 using calculated  $\text{NO}_3$  concentrations from the equilibrium between  $\text{NO}_3$  and  $\text{N}_2\text{O}_5$   
356 (Figure S5) also indicates that uncertainties in  $\text{NO}_3$  measurements cannot account for the  
357 discrepancies between measured and modeled phenol at night. The high phenol  
358 concentrations measured at night might be a result of primary emissions. Indeed, the  
359 measured phenol concentration was slightly enhanced in the plume with high methane  
360 concentrations (see Figure 4A). However, a simulation using the measured phenol  
361 concentrations as a constraint in the box model, predicted much higher NP concentrations  
362 than measurements (Figure S4). Perhaps a more likely explanation for the enhanced  
363 phenol concentrations at night is that the measurements of phenol by PTR-TOF suffer  
364 from chemical interferences at night. Vinylfuran might be a candidate (Karl et al.,

365 2007;Stockwell et al., 2015). Thus, the modeled concentrations of phenol shown in  
366 Figure 5 will be used in the following discussions.

### 367 3.2.2 NO<sub>2</sub> dependence of NP yields

368 As shown in Figure 1, NP is generated from the reaction of NO<sub>2</sub> with phenoxy  
369 radicals (C<sub>6</sub>H<sub>5</sub>O·) (Berndt and Boge, 2003), which is an intermediate from the reactions  
370 of OH and NO<sub>3</sub> radicals with phenol and the reaction of phenylperoxy radicals (C<sub>6</sub>H<sub>5</sub>O<sub>2</sub>)  
371 with NO. In addition to NO<sub>2</sub>, C<sub>6</sub>H<sub>5</sub>O· radicals also react with NO and O<sub>3</sub> (Platz et al.,  
372 1998) (see Figure 1). Thus, the yield of NP has been reported to depend on NO<sub>2</sub>  
373 concentrations in the atmosphere (Berndt and Boge, 2003).

374 In the MCM v3.2, only the reactions of C<sub>6</sub>H<sub>5</sub>O radical with O<sub>3</sub> and NO<sub>2</sub> are  
375 included and here we added the reaction of C<sub>6</sub>H<sub>5</sub>O with NO ( $k=1.88\times 10^{-12}$  cm<sup>3</sup> molecule<sup>-1</sup>  
376 s<sup>-1</sup>) for a new simulation. Compared to the base simulation, the modeled concentrations  
377 of NP are lower, especially for the period of 11:00-17:00, as the effective yield of NP is  
378 reduced (Figure 5). The small enhancement during the period of 11:00-17:00 in NP  
379 concentrations from the base simulation is absent in the simulation with the reaction of  
380 C<sub>6</sub>H<sub>5</sub>O with NO. The variations of modeled NP concentrations in the daytime from the  
381 new simulation are in better agreement with the measurements (Figure 5). This indicates  
382 the reaction of NO and C<sub>6</sub>H<sub>5</sub>O radical should be considered to account for the NO<sub>2</sub>  
383 dependence of NP formation.

384 Another simulation using fixed NP yields from phenol oxidation reported in  
385 Atkinson et al. (1992) (6.7% for OH oxidation and 25.1% for NO<sub>3</sub> oxidation) is also  
386 performed. This simulation neglects any dependence of NP yield from phenol oxidation  
387 on concentrations of NO<sub>2</sub>, O<sub>3</sub> and NO. We observed lower concentrations during both the  
388 day and night compared to the base simulation (Figure 5). However, the enhancement of  
389 modeled NP in the period of 11:00 -17:00 is distinctly observed with the simulation using  
390 the fixed yields in Atkinson et al. (1992), which is in contrast to the lowest concentration  
391 in the afternoon from our observations. This, again, indicates there must be a dependence  
392 of NP yield from phenol oxidation on NO<sub>2</sub> concentrations in the atmosphere.

### 393 3.2.3 Gas-particle partitioning of NP

394 NP formed in the gas phase can partition into particles (Harrison et al., 2005a).  
395 Measurements in several studies demonstrated that 2-NP and MNP were mainly found in  
396 the gas phase (Herterich and Herrmann, 1990; Cecinato et al., 2005; Morville et al., 2006).  
397 However, the reported particle fractions of 4-NP and DNP exhibit a broad range in  
398 values: the particle fractions of 4-NP and DNP reported in Herterich and Herrmann  
399 (1990) were both lower than 15%, whereas most of the concentrations of 4-NP (>75%)  
400 (Cecinato et al., 2005) and DNP (>95%) (Morville et al., 2006) were detected in particles  
401 in these two studies.

402 The concentrations of NP and other nitrated phenols in particles were not measured  
403 in this study. We acknowledge that some fractions of nitrated phenols in particles may  
404 evaporate into gas phase in the heated inlets. If it holds true, the measured concentrations  
405 of nitrated phenols in this study would fall somewhere between concentrations in gas-  
406 phase and the total gas+particle concentrations. Here, the gas-particle partitioning of NP  
407 as a function of time was estimated using the equilibrium absorption partitioning theory  
408 (Pankow, 1994; Donahue et al., 2006) (see details in the SI), based upon pure-compound  
409 liquid vapor pressures of 2-NP and 4-NP (Schwarzenbach et al., 1988) (Table 2) and  
410 organic aerosol (OA) concentrations measured with an aerosol mass spectrometer  
411 (AMS). The dependence with temperature was accounted for using the Clausius-  
412 Clapeyron relationship with reported enthalpies of evaporation ( $H_{\text{vap}}$ ) (Schwarzenbach et  
413 al., 1988). Although vapor pressures from Schwarzenbach et al. (1988) might have  
414 significant uncertainties, Schwarzenbach et al. (1988) provided the only comprehensive  
415 measurements of sub-cooled liquid vapor pressures of nitrated phenols in the literature.

416 The calculated fractions in particle ( $F_p$ ) for 2-NP were generally very low (campaign  
417 average:  $1.1 \pm 0.9 \times 10^{-4}$ , max:  $7.3 \times 10^{-4}$ ), whereas  $F_p$  for 4-NP were higher (average:  
418  $0.053 \pm 0.048$ , max: 0.38). The variability of the determined  $F_p$  values is the result of  
419 variations of both OA concentrations ( $12.5 \pm 8.7 \mu\text{g}/\text{m}^3$ , min:  $<1 \mu\text{g}/\text{m}^3$ , max:  $42.6 \mu\text{g}/\text{m}^3$ )  
420 and ambient temperature ( $-5 \pm 5 \text{ }^\circ\text{C}$ , min:  $-17 \text{ }^\circ\text{C}$ , max:  $10 \text{ }^\circ\text{C}$ ) during the campaign. The  
421 higher  $F_p$  for 4-NP is expected, as 4-NP ( $1.4 \times 10^{-3}$  Torr at 298 K) has much lower vapor  
422 pressure than 2-NP (0.20 Torr at 298 K) (Table 2). In addition to absorption, partitioning  
423 of NP into the aqueous phase of particles is another possible pathway affecting  $F_p$ . This  
424 mechanism is estimated using Henry's law constants (Sander, 2015) and the liquid water

425 content (LWC) ( $8.4 \pm 7.5 \mu\text{g}/\text{m}^3$ ) in aerosol determined using the ISORROPIA model  
 426 (Fountoukis and Nenes, 2007). The estimated  $F_p$  values based on aqueous phase  
 427 partitioning for 2-NP ( $1.3 \times 10^{-7}$ ) and 4-NP ( $3.0 \times 10^{-5}$ ) are both much lower than  $F_p$   
 428 estimated from the equilibrium absorption partitioning theory, indicating partitioning of  
 429 NP into the particle aqueous phase was not important during UBWOS 2014.

430 The gas-particle partitioning of 2-NP and 4-NP determined above was incorporated  
 431 into the box model by constraining the estimated  $F_p$  in the determination of gas-particle  
 432 mass transport rates. The mass transport rates ( $R_{in}$  and  $R_{out}$ ) of a species into and out of  
 433 particles with radius  $r$  are approximated by (Jacob, 2000):

$$R_{in} = \left( \frac{r}{D_g} + \frac{4}{v\alpha} \right)^{-1} A \times c_g = \frac{1}{\tau} \times c_g \quad (1)$$

$$R_{out} = \left( \frac{r}{D_g} + \frac{4}{v\alpha} \right)^{-1} A \times \frac{c_p}{K_{ep}} = \frac{1}{\tau} \times \frac{c_p}{K_{ep}} \quad (2)$$

434 where  $c_g$  and  $c_p$  are concentrations of the species in the gas and particle phase.  $D_g$   
 435 is the gas-phase molecular diffusion coefficient ( $\text{m}^2 \text{s}^{-1}$ ),  $v$  is the mean molecular speed  
 436 ( $\text{m s}^{-1}$ ),  $\alpha$  is the mass accommodation coefficient.  $A$  is the aerosol surface area per unit  
 437 volume of air ( $\text{m}^2 \text{m}^{-3}$ ).  $K_{ep}$  is the equilibrium constant, i.e.  $c_p/c_g$ , or  $/(1 - F_p)$ . The  
 438 characteristic time scale of mass transfer ( $\tau$ ) is estimated to be on the order of minutes for  
 439 particles in the troposphere (Bowman et al., 1997; Jacob, 2000). Thus, rather than  
 440 determining the characteristic time scale explicitly, we assume that the equilibrium is  
 441 maintained at each model step ( $\tau=5$  min). After entering into particles, no further reaction  
 442 of NP was prescribed in the model. The modeled diurnal profiles of NP associated with  
 443 the inclusion of gas-particle partitioning are shown in Figure 6. Compared to the base  
 444 simulation, the modeled NP concentrations in the gas phase using the estimated  $F_p$  from  
 445 4-NP are lower (4-8%) for most of the day and slightly higher (2-3%) in the morning  
 446 when NP concentrations decreased quickly. Since the predicted  $F_p$  from 2-NP is very  
 447 small, the modeled NP concentrations in the gas phase using the estimates from 2-NP  
 448 were almost identical to the base simulation. In contrast with the modeled concentrations  
 449 of NP in the gas phase, the modeled total concentrations of NP in gas and particle phase  
 450 are consistently higher than the base simulation that does not consider gas-particle

451 partitioning. In summary, we observe relatively small changes of the modeled gaseous  
452 NP concentrations after the inclusion of gas-particle partitioning in the box model.  
453 Further measurements of the gas/particle partitioning of nitrated phenols are needed to  
454 explain the variety of  $F_p$  values observed in different studies and/or the potential  
455 differences between measurements and prediction from the equilibrium absorption  
456 partitioning model.

#### 457 3.2.4 Budget analysis of phenol and nitrophenol

458 Diurnal profiles of formation and loss rates derived from the base simulation of the  
459 box model for both phenol and NP are shown in Figure 7. Production of phenol only  
460 occurs in the daytime from OH oxidation of benzene. The magnitudes of losses of phenol  
461 due to OH oxidation (21 ppt/day) and  $\text{NO}_3$  oxidation (19 ppt/day) are comparable on a  
462 daily basis. From morning to afternoon (8:00-15:00), production of phenol is larger than  
463 the losses, resulting in continuous growth of phenol concentrations in this period. After  
464 15:00 pm, the losses start to surpass the production and phenol concentrations decrease  
465 quickly. With fast reduction of phenol concentrations in the evening, phenol loss from the  
466 reaction with  $\text{NO}_3$  mainly occurred before midnight.

467 As shown in Figure 7, NP is produced during both daytime and night, with more  
468 production in the daytime. As mentioned earlier, the only formation pathway of NP is  
469 from the reaction of phenoxy radicals ( $\text{C}_6\text{H}_5\text{O}$ ) with  $\text{NO}_2$ , so the contribution from  
470 different pathways to NP formation can be derived from source analysis of  $\text{C}_6\text{H}_5\text{O}$   
471 radicals (Figure 7C). The production of  $\text{C}_6\text{H}_5\text{O}$  radicals is dominated by the reaction of  
472  $\text{C}_6\text{H}_5\text{O}_2$  radicals with NO during daytime (71% for 24-hour average) and the reaction of  
473 phenol with  $\text{NO}_3$  radicals at night (27% for 24-hour average). There are several sources  
474 contributing to the formation of  $\text{C}_6\text{H}_5\text{O}_2$  radicals in the MCM, including photolysis of  
475 benzaldehyde and peroxybenzoic acid, OH oxidation of benzoic acid and phenyl  
476 hydroperoxide, and degradations of other radicals (e.g., phenylperoxyacyl radical  
477  $\text{C}_6\text{H}_5\text{CO}_3$ ), suggesting a wide range of aromatic compounds as the precursors of NP in  
478 the daytime. The reaction of phenol with OH radicals only accounts for a small fraction  
479 of the production of  $\text{C}_6\text{H}_5\text{O}$  radicals (2% for 24-hour average), due to the small yield of  
480 NP (6%) from the reaction of OH with phenol in the MCM. This indicates phenol is not

481 an important precursor for NP during daytime. The destruction of NP is mainly due to  
482 photolysis (17 ppt/day), with some contributions from NO<sub>3</sub> reaction (1.7 ppt/day). The  
483 reaction with OH radicals is not important for the losses of NP in the UBWOS 2014.  
484 Dilution/deposition processes account for 20% of the total loss of NP in the box model.  
485 Our results are consistent with a previous proposal on photolysis as the dominant  
486 chemical loss pathway for nitrated phenols (Bejan et al., 2007). Based on the conditions  
487 at the Horse Pool site, the lifetime of NP due to photolysis at noontime is calculated to be  
488 ~80 min. As the result of the short lifetime of NP during daytime, the production (23.6  
489 ppt/day) and loss rates (23.1 ppt/day) of NP maintain a balanced budget of NP on a daily  
490 basis. The inclusion of the reaction of phenoxy radicals (C<sub>6</sub>H<sub>5</sub>O) with NO discussed in  
491 Section 3.2.2 would mainly affect the NP budget at midday, with smaller production and  
492 loss in this period.

493 The different diurnal variations of production and loss rates of NP explain the  
494 measured diurnal profile of NP concentrations shown in Figure 3. The increase of loss  
495 rates from photolysis result in the quick decline of NP concentrations in the morning. The  
496 formation of NP from NO<sub>3</sub> oxidation of phenol in the evening exceeds the destruction of  
497 NP, which accounts for the enhancement of NP in this period. The formation and loss  
498 rates of NP are comparable in the afternoon and relatively constant concentrations of NP  
499 were observed.

500 A previous study showed that photolysis of nitrated phenols contributes to HONO  
501 formation (Bejan et al., 2006). If we assume photolysis of nitrated phenols at rates of  
502 1.4%×J(NO<sub>2</sub>) yields HONO at a 100% yield (upper limit), photolysis of NP, MNP and  
503 DMNP together accounted for a formation rate of HONO of 1.5±1.9 ppt/hour around  
504 noontime (9:00-15:00) during UBWOS 2014. This photolysis source would increase the  
505 steady state concentrations of HONO by 0.5 ppt in early morning (7:00-8:30) and 0.2 ppt  
506 during the noontime period (9:00-15:00), which are only small fractions of measured  
507 HONO concentrations (50-100 ppt) during UBWOS 2014 (Edwards et al., 2014).

### 508 **3.3 Dinitrophenol**

509 Further oxidation of NP in the presence of NO<sub>x</sub> produces DNP. The measured time  
510 series of DNP in January 18-22 is shown in Figure 8. A similar diurnal profile was

511 observed for DNP as other nitrated phenols, with higher concentrations at night and lower  
512 in the daytime. We also notice that the peak time of DNP concentrations at night was  
513 somewhat later than NP, consistent with further oxidation of NP as the source of DNP.

514 In the MCM v3.2, reactions of NP with OH or NO<sub>3</sub> radicals generate nitrophenoxy  
515 radicals (NO<sub>2</sub>C<sub>6</sub>H<sub>5</sub>O·), which react further with NO<sub>2</sub> to form DNP. Here, we assume  
516 DNP has the same photolysis rate as NP (1.4% of photolysis frequency of NO<sub>2</sub>) (Bardini,  
517 2006) and we added the photolysis into the MCM v3.2. The simulated concentrations of  
518 DNP from the box model are also displayed in Figure 8. The agreement between  
519 measurements and simulation is quite good from the base simulation. DNP has also been  
520 observed in the particle phase at significant fractions (Morville et al., 2006). Using the  
521 equilibrium absorption partitioning theory described in Section 3.3.3 and vapor pressures  
522 of two different DNP isomers (2,4-DNP and 2,5-DNP) (Table 2), we incorporated the  
523 calculated particle fractions of DNP (Table 2) into the box model as a sensitivity  
524 simulation. The predicted DNP concentrations from this simulation are around 5% lower  
525 than the base simulation at night. Considering the limited information on DNP formation,  
526 the agreement between measured and modeled concentrations of DNP from both  
527 simulations is encouraging. This degree of agreement implies that DNP concentrations  
528 measured in UBWOS 2014 are explainable by known chemical reactions in the gas  
529 phase.

530 As described in Section 3.2, photolysis is the dominant sink for NP and box  
531 model results indicate that photolysis of NP may not generate phenoxy radical (by losing  
532 NO<sub>2</sub>). The other possible product from photolysis of NP is nitrophenoxy radical (Figure 1  
533 Route 3), which would act as a secondary source of DNP. This assumption is evaluated  
534 as a new simulation. The simulation predicted concentration peaks of DNP in the  
535 morning (the orange line in Figure 8), which are not observed in our measurements.  
536 Thus, we exclude nitrophenoxy radical as the main products of photolysis of NP.  
537 However, the product and exact chemical mechanisms for photolysis of NP remain  
538 unclear and thus the photolysis of NP warrants further detailed studies.

### 539 **3.4 Non-gas phase reactions**

540 The box model only considers gas phase reactions that produce nitrated phenols. In  
541 addition to gas phase reactions, aqueous reactions in particles and heterogeneous  
542 reactions are other potential sources of nitrated phenols (Harrison et al., 2005a). As  
543 shown in Section 3.3.3, using chemical compositions of aerosol at the Horse Pool site and  
544 the ISORROPIA model (Fountoukis and Nenes, 2007), the liquid water content (LWC) in  
545 aerosol during UBWOS 2014 was estimated to be  $8.4 \pm 7.5 \mu\text{g}/\text{m}^3$  (whole campaign  
546 average), or  $8.4 \pm 7.5 \times 10^{-12}$  expressed as the volume fraction. Based on the box modeling  
547 results in Harrison et al. (2005b), aqueous reactions contribute less than 2% of NP  
548 production at  $3 \times 10^{-9}$  volume fraction LWC. Thus, aqueous reactions in UBWOS 2014  
549 should not be a significant source for nitrated phenols compared to gas phase reactions.

550 The Uintah Basin was covered by snow during UBWOS 2014. The importance of  
551 heterogeneous reactions on the snow surface to formation of nitrated phenols is evaluated  
552 using measurements of the vertical gradients of these species. Here, the concentration  
553 gradient is defined as the concentrations measured at 18.5 m subtracted from those  
554 measured at 1 m. As shown in Figure 9, we observed negative concentration gradients for  
555 nitrated phenols at night, indicating that deposition was playing a role and consequently  
556 ground snow was a net sink for nitrated phenols at night. A previous study suggested  
557 heterogeneous reaction of  $\text{N}_2\text{O}_5$  with phenol in the aqueous phase produces NP (Heal et  
558 al., 2007). Strong deposition of  $\text{N}_2\text{O}_5$  to the snow surface was observed at night during  
559 UBWOS 2014, but as discussed no production of nitrated phenols near the snow surface  
560 was detected at night (Figure 9). The vertical gradients for nitrated phenols in the daytime  
561 fluctuated around zero with large variations, which might be a result of their low  
562 concentrations during daytime. The analysis of vertical gradients implies that  
563 heterogeneous reactions on snow surface may not be important for formation of nitrated  
564 phenols in the atmosphere during UBWOS 2014.

#### 565 **4. Conclusions**

566 In this study, nitrated phenols in the gas phase were measured using an online  
567 acetate ToF-CIMS in an oil and gas production region during winter. Strong diurnal  
568 profiles were observed for nitrated phenols, with concentration maxima at night. As the  
569 dominant sink for nitrated phenols, photolysis accounted for lower concentrations of

570 nitrated phenols during daytime. We determined that the photolysis of nitrated phenols  
571 was not an important source of HONO during UBWOS 2014. Based on box model  
572 results, NP was mainly formed in the daytime (73%) from a wide range of precursors,  
573 with significant contribution from the reaction of phenol with NO<sub>3</sub> radicals at night  
574 (27%). Box model results also indicated that gas phase oxidation of aromatics was able to  
575 explain the measured concentrations of NP and DNP. We demonstrated that box model  
576 results provided valuable information on the detailed chemical mechanisms in the  
577 formation and destruction of NP, e.g., the NO<sub>2</sub> dependence of NP yields from phenol  
578 oxidations and chemical products of NP photolysis. We determined that aqueous-phase  
579 reactions and heterogeneous reactions were minor sources of nitrated phenols in this  
580 study. Although the dataset of nitrated phenols was collected in an oil and gas production  
581 region, the chemistry in secondary formation of nitrated phenols and the dynamics of the  
582 budget of nitrated phenols in other regions, e.g., urban areas, should behave similarly to  
583 those shown in this study.

584 Biomass burning activity did not affect the UBWOS 2014 measurements, and the  
585 concentrations of phenols and nitrated phenols were mainly from oxidations of aromatics  
586 in the atmosphere. The measurements during UBWOS 2014 provided a great opportunity  
587 to study secondary formation of nitrated phenols in the absence of other confounding  
588 sources. The UBWOS 2014 campaign also represented the first coincident and high time-  
589 resolution measurements of aromatic hydrocarbons, phenols and nitrated phenols in  
590 ambient air. The measurements of phenol and nitrated phenols provided a better  
591 understanding of their sources, budgets and roles in atmospheric chemistry and for the  
592 evaluation of the oxidation mechanisms of aromatics. This is achieved by the emergence  
593 of the new ToF-CIMS and PTR-TOF techniques. We envision that these techniques will  
594 provide the ability to detect many other intermediate compounds in the atmosphere and  
595 that the measurements will advance the understanding of atmospheric oxidation  
596 processes.

597

## 598 **Acknowledgement**

599 The Uintah Basin Winter Ozone Studies were a joint project led and coordinated by the

600 Utah Department of Environmental Quality (UDEQ) and supported by the Uintah Impact  
601 Mitigation Special Service District (UIMSSD), the Bureau of Land Management (BLM),  
602 the Environmental Protection Agency (EPA) and Utah State University. This work was  
603 funded in part by the Western Energy Alliance, and NOAA's Atmospheric Chemistry,  
604 Climate and Carbon Cycle program. We thank Questar Energy Products for site  
605 preparation and support. Chemical compositions of aerosol were provided by Tim Bates  
606 and James Johnson from NOAA Pacific Marine Environmental Laboratory (PMEL) and  
607 the Joint Institute for the Study of the Atmosphere and Ocean (JISAO) at University of  
608 Washington.  
609

## 610 **References:**

- 611 Atkinson, R., Aschmann, S. M., and Arey, J.: Reactions of hydroxyl and nitrogen trioxide  
612 radicals with phenol, cresols, and 2-nitrophenol at  $296 \pm 2$  K, *Environmental Science &*  
613 *Technology*, 26, 1397-1403, 10.1021/es00031a018, 1992.
- 614 Bardini, P.: *Atmospheric Chemistry of Dimethylphenols & Nitrophenols*, PhD,  
615 University College Cork, Corcaigh, 2006.
- 616 Bartmess, J. E.: Negative Ion Energetics Data, NIST Chemistry WebBook, NIST  
617 Standard Reference Database Number 69, edited by: Linstrom, P. J., and Mallard, W.  
618 G., National Institute of Standards and Technology, Gaithersburg MD, 20899  
619 <http://webbook.nist.gov>, (retrieved August 28, 2015). 2015.
- 620 Bejan, I., Abd El Aal, Y., Barnes, I., Benter, T., Bohn, B., Wiesen, P., and Kleffmann, J.:  
621 The photolysis of ortho-nitrophenols: a new gas phase source of HONO, *Phys Chem*  
622 *Chem Phys*, 8, 2028-2035, 2006.
- 623 Bejan, I., Barnes, I., Olariu, R., Zhou, S., Wiesen, P., and Benter, T.: Investigations on  
624 the gas-phase photolysis and OH radical kinetics of methyl-2-nitrophenols, *Phys Chem*  
625 *Chem Phys*, 9, 5686-5692, 10.1039/B709464G, 2007.
- 626 Bejan, I., Duncianu, M., Olariu, R., Barnes, I., Seakins, P. W., and Wiesen, P.: Kinetic  
627 Study of the Gas-Phase Reactions of Chlorine Atoms with 2-Chlorophenol, 2-  
628 Nitrophenol, and Four Methyl-2-nitrophenol Isomers, *The Journal of Physical*  
629 *Chemistry A*, 119, 4735-4745, 10.1021/acs.jpca.5b02392, 2015.
- 630 Berndt, T., and Boge, O.: Gas-phase reaction of OH radicals with phenol, *Phys Chem*  
631 *Chem Phys*, 5, 342-350, 10.1039/B208187C, 2003.
- 632 Bertram, T. H., Kimmel, J. R., Crisp, T. A., Ryder, O. S., Yatavelli, R. L. N., Thornton, J.  
633 A., Cubison, M. J., Gonin, M., and Worsnop, D. R.: A field-deployable, chemical  
634 ionization time-of-flight mass spectrometer, *Atmos. Meas. Tech.*, 4, 1471-1479,  
635 10.5194/amt-4-1471-2011, 2011.
- 636 Bolzacchini, E., Bruschi, M., Hjorth, J., Meinardi, S., Orlandi, M., Rindone, B., and  
637 Rosenbohm, E.: Gas-Phase Reaction of Phenol with NO<sub>3</sub>, *Environmental Science &*  
638 *Technology*, 35, 1791-1797, 10.1021/es001290m, 2001.
- 639 Bowman, F. M., Odum, J. R., Seinfeld, J. H., and Pandis, S. N.: Mathematical model for  
640 gas-particle partitioning of secondary organic aerosols, *Atmospheric Environment*, 31,  
641 3921-3931, [http://dx.doi.org/10.1016/S1352-2310\(97\)00245-8](http://dx.doi.org/10.1016/S1352-2310(97)00245-8), 1997.
- 642 Brophy, P., and Farmer, D. K.: A switchable reagent ion high resolution time-of-flight  
643 chemical ionization mass spectrometer for real-time measurement of gas phase  
644 oxidized species: characterization from the 2013 southern oxidant and aerosol study,  
645 *Atmospheric Measurement Techniques*, 8, 2945-2959, 10.5194/amt-8-2945-2015,  
646 2015.
- 647 Cappellin, L., Karl, T., Probst, M., Ismailova, O., Winkler, P. M., Soukoulis, C., Aprea,  
648 E., Mark, T. D., Gasperi, F., and Biasioli, F.: On quantitative determination of volatile  
649 organic compound concentrations using proton transfer reaction time-of-flight mass  
650 spectrometry, *Environ Sci Technol*, 46, 2283-2290, 10.1021/es203985t, 2012.
- 651 Caralp, F., Foucher, V., Lesclaux, R., J. Wallington, T., and D. Hurley, M.: Atmospheric  
652 chemistry of benzaldehyde: UV absorption spectrum and reaction kinetics and  
653 mechanisms of the C<sub>6</sub>H<sub>5</sub>C(O)O<sub>2</sub> radical, *Phys Chem Chem Phys*, 1, 3509-3517,  
654 10.1039/A903088C, 1999.

655 Cecinato, A., Di Palo, V., Pomata, D., Tomasi Scianò, M. C., and Possanzini, M.:  
656 Measurement of phase-distributed nitrophenols in Rome ambient air, *Chemosphere*, 59,  
657 679-683, <http://dx.doi.org/10.1016/j.chemosphere.2004.10.045>, 2005.

658 Chen, J., Wenger, J. C., and Venables, D. S.: Near-Ultraviolet Absorption Cross Sections  
659 of Nitrophenols and Their Potential Influence on Tropospheric Oxidation Capacity,  
660 *The Journal of Physical Chemistry A*, 115, 12235-12242, 10.1021/jp206929r, 2011.

661 Cheng, S.-B., Zhou, C.-H., Yin, H.-M., Sun, J.-L., and Han, K.-L.: OH produced from o-  
662 nitrophenol photolysis: A combined experimental and theoretical investigation, *The*  
663 *Journal of Chemical Physics*, 130, 234311,  
664 doi:<http://dx.doi.org/10.1063/1.3152635>, 2009.

665 Corbin, J., Othman, A., D. Allan, J., R. Worsnop, D., D. Haskins, J., Sierau, B.,  
666 Lohmann, U., and A. Mensah, A.: Peak-fitting and integration imprecision in the  
667 Aerodyne aerosol mass spectrometer: effects of mass accuracy on location-constrained  
668 fits, *Atmospheric Measurement Techniques*, 8, 4615-4636, 10.5194/amt-8-4615-2015,  
669 2015.

670 Cubison, M. J., and Jimenez, J. L.: Statistical precision of the intensities retrieved from  
671 constrained fitting of overlapping peaks in high-resolution mass spectra, *Atmospheric*  
672 *Measurement Techniques*, 8, 2333-2345, 10.5194/amt-8-2333-2015, 2015.

673 de Gouw, J., and Warneke, C.: Measurements of volatile organic compounds in the  
674 earth's atmosphere using proton-transfer-reaction mass spectrometry, *Mass*  
675 *Spectrometry Reviews*, 26, 223-257, 2007.

676 Delhomme, O., Morville, S., and Millet, M.: Seasonal and diurnal variations of  
677 atmospheric concentrations of phenols and nitrophenols measured in the Strasbourg  
678 area, France, *Atmospheric Pollution Research*, 16-22, 10.5094/APR.2010.003, 2010.

679 Desyaterik, Y., Sun, Y., Shen, X., Lee, T., Wang, X., Wang, T., and Collett, J. L.:  
680 Speciation of "brown" carbon in cloud water impacted by agricultural biomass burning  
681 in eastern China, *Journal of Geophysical Research: Atmospheres*, 118, 7389-7399,  
682 10.1002/jgrd.50561, 2013.

683 Donahue, N. M., Robinson, A. L., Stanier, C. O., and Pandis, S. N.: Coupled Partitioning,  
684 Dilution, and Chemical Aging of Semivolatile Organics, *Environmental Science &*  
685 *Technology*, 40, 2635-2643, 10.1021/es052297c, 2006.

686 Dubé, W. P., Brown, S. S., Osthoff, H. D., Nunley, M. R., Ciciora, S. J., Paris, M. W.,  
687 McLaughlin, R. J., and Ravishankara, A. R.: Aircraft instrument for simultaneous, in  
688 situ measurement of NO<sub>3</sub> and N<sub>2</sub>O<sub>5</sub> via pulsed cavity ring-down spectroscopy, *Review*  
689 *of Scientific Instruments*, 77, 034101, doi:<http://dx.doi.org/10.1063/1.2176058>,  
690 2006.

691 Edwards, P. M., Brown, S. S., Roberts, J. M., Ahmadov, R., Banta, R. M., deGouw, J. A.,  
692 Dube, W. P., Field, R. A., Flynn, J. H., Gilman, J. B., Graus, M., Helmig, D., Koss, A.,  
693 Langford, A. O., Lefer, B. L., Lerner, B. M., Li, R., Li, S. M., McKeen, S. A., Murphy,  
694 S. M., Parrish, D. D., Senff, C. J., Soltis, J., Stutz, J., Sweeney, C., Thompson, C. R.,  
695 Trainer, M. K., Tsai, C., Veres, P. R., Washenfelder, R. A., Warneke, C., Wild, R. J.,  
696 Young, C. J., Yuan, B., and Zamora, R.: High winter ozone pollution from carbonyl  
697 photolysis in an oil and gas basin, *Nature*, 514, 351-354, 10.1038/nature13767, 2014.

698 Fernandez, P., Grifoll, M., Solanas, A. M., Bayona, J. M., and Albaiges, J.: Bioassay-  
699 directed chemical analysis of genotoxic components in coastal sediments,  
700 *Environmental Science & Technology*, 26, 817-829, 10.1021/es00028a024, 1992.

701 Fountoukis, C., and Nenes, A.: ISORROPIA II: a computationally efficient  
702 thermodynamic equilibrium model for  $K^+$   $Ca^{2+}$   $Mg^{2+}$   $NH_4^+$   $Na^+$   $SO_4^{2-}$   $NO_3^-$   $Cl^-$   
703  $H_2O$  aerosols, *Atmos. Chem. Phys.*, 7, 4639-4659, 10.5194/acp-7-4639-2007, 2007.

704 Gilman, J. B., Lerner, B. M., Kuster, W. C., and de Gouw, J. A.: Source signature of  
705 volatile organic compounds from oil and natural gas operations in northeastern  
706 Colorado, *Environ Sci Technol*, 47, 1297-1305, 10.1021/es304119a, 2013.

707 Harrison, M. A. J., Barra, S., Borghesi, D., Vione, D., Arsene, C., and Iulian Olariu, R.:  
708 Nitrated phenols in the atmosphere: a review, *Atmospheric Environment*, 39, 231-248,  
709 <http://dx.doi.org/10.1016/j.atmosenv.2004.09.044>, 2005a.

710 Harrison, M. A. J., Heal, M. R., and Cape, J. N.: Evaluation of the pathways of  
711 tropospheric nitrophenol formation from benzene and phenol using a multiphase  
712 model, *Atmos. Chem. Phys.*, 5, 1679-1695, 10.5194/acp-5-1679-2005, 2005b.

713 Heal, M. R., Harrison, M. A. J., and Neil Cape, J.: Aqueous-phase nitration of phenol by  
714  $N_2O_5$  and  $ClNO_2$ , *Atmospheric Environment*, 41, 3515-3520,  
715 <http://dx.doi.org/10.1016/j.atmosenv.2007.02.003>, 2007.

716 Herterich, R., and Herrmann, R.: Comparing the distribution of nitrated phenols in the  
717 atmosphere of two German hill sites, *Environ Technol*, 11, 961-972,  
718 10.1080/09593339009384948, 1990.

719 Inomata, S., Tanimoto, H., Fujitani, Y., Sekimoto, K., Sato, K., Fushimi, A., Yamada, H.,  
720 Hori, S., Kumazawa, Y., Shimono, A., and Hikida, T.: On-line measurements of  
721 gaseous nitro-organic compounds in diesel vehicle exhaust by proton-transfer-reaction  
722 mass spectrometry, *Atmospheric Environment*, 73, 195-203,  
723 <http://dx.doi.org/10.1016/j.atmosenv.2013.03.035>, 2013.

724 Jacob, D. J.: Heterogeneous chemistry and tropospheric ozone, *Atmospheric*  
725 *Environment*, 34, 2131-2159, [http://dx.doi.org/10.1016/S1352-2310\(99\)00462-8](http://dx.doi.org/10.1016/S1352-2310(99)00462-8),  
726 2000.

727 Jenkin, M. E., Saunders, S. M., Wagner, V., and Pilling, M. J.: Protocol for the  
728 development of the Master Chemical Mechanism, MCM v3 (Part B): tropospheric  
729 degradation of aromatic volatile organic compounds, *Atmos. Chem. Phys.*, 3, 181-193,  
730 10.5194/acp-3-181-2003, 2003.

731 Jenkin, M. E., Wyche, K. P., Evans, C. J., Carr, T., Monks, P. S., Alfarra, M. R., Barley,  
732 M. H., McFiggans, G. B., Young, J. C., and Rickard, A. R.: Development and chamber  
733 evaluation of the MCM v3.2 degradation scheme for  $\beta$ -caryophyllene, *Atmos. Chem.*  
734 *Phys.*, 12, 5275-5308, 10.5194/acp-12-5275-2012, 2012.

735 Karl, T. G., Christian, T. J., Yokelson, R. J., Artaxo, P., Hao, W. M., and Guenther, A.:  
736 The Tropical Forest and Fire Emissions Experiment: method evaluation of volatile  
737 organic compound emissions measured by PTR-MS, FTIR, and GC from tropical  
738 biomass burning, *Atmospheric Chemistry and Physics*, 7, 5883-5897, 2007.

739 Kaser, L., Karl, T., Guenther, A., Graus, M., Schnitzhofer, R., Turnipseed, A., Fischer,  
740 L., Harley, P., Madronich, M., Gochis, D., Keutsch, F. N., and Hansel, A.: Undisturbed  
741 and disturbed above canopy ponderosa pine emissions: PTR-TOF-MS measurements  
742 and MEGAN 2.1 model results, *Atmos. Chem. Phys.*, 13, 11935-11947, 2013.

743 Kitanovski, Z., Grgić, I., Yasmeen, F., Claeys, M., and Čusak, A.: Development of a  
744 liquid chromatographic method based on ultraviolet-visible and electrospray ionization  
745 mass spectrometric detection for the identification of nitrocatechols and related tracers

746 in biomass burning atmospheric organic aerosol, *Rapid Communications in Mass*  
747 *Spectrometry*, 26, 793-804, 10.1002/rcm.6170, 2012.

748 Lauraguais, A., Coeur-Tourneur, C., Cassez, A., Deboudt, K., Fourmentin, M., and  
749 Choël, M.: Atmospheric reactivity of hydroxyl radicals with guaiacol (2-  
750 methoxyphenol), a biomass burning emitted compound: Secondary organic aerosol  
751 formation and gas-phase oxidation products, *Atmospheric Environment*, 86, 155-163,  
752 <http://dx.doi.org/10.1016/j.atmosenv.2013.11.074>, 2014.

753 Lee, B. H., Lopez-Hilfiker, F., Mohr, C., Kurtén, T. C., Worsnop, D., and Thornton, J.  
754 A.: An Iodide-Adduct High-Resolution Time-of-Flight Chemical-Ionization Mass  
755 Spectrometer: Application to Atmospheric Inorganic and Organic Compounds,  
756 *Environmental Science & Technology*, 10.1021/es500362a, 2014.

757 Lin, P., Liu, J., Shilling, J. E., Kathmann, S., Laskin, J., and Laskin, A.: Molecular  
758 Characterization of Brown Carbon (BrC) Chromophores in Secondary Organic Aerosol  
759 Generated From Photo-Oxidation of Toluene, *Phys Chem Chem Phys*,  
760 10.1039/C5CP02563J, 2015.

761 Mohr, C., Lopez-Hilfiker, F. D., Zotter, P., Prévôt, A. S. H., Xu, L., Ng, N. L., Herndon,  
762 S. C., Williams, L. R., Franklin, J. P., Zahniser, M. S., Worsnop, D. R., Knighton, W.  
763 B., Aiken, A. C., Gorkowski, K. J., Dubey, M. K., Allan, J. D., and Thornton, J. A.:  
764 Contribution of Nitrated Phenols to Wood Burning Brown Carbon Light Absorption in  
765 Detling, United Kingdom during Winter Time, *Environmental Science & Technology*,  
766 47, 6316-6324, 10.1021/es400683v, 2013.

767 Morville, S., Scheyer, A., Mirabel, P., and Millet, M.: Spatial and Geographical  
768 Variations of Urban, Suburban and Rural Atmospheric Concentrations of Phenols and  
769 Nitrophenols (7 pp), *Environ Sci Pollut R*, 13, 83-89, 10.1065/espr2005.06.264, 2006.

770 Müller, M., George, C., and D'Anna, B.: Enhanced spectral analysis of C-TOF Aerosol  
771 Mass Spectrometer data: Iterative residual analysis and cumulative peak fitting,  
772 *International Journal of Mass Spectrometry*, 306, 1-8,  
773 <http://dx.doi.org/10.1016/j.ijms.2011.04.007>, 2011.

774 Natangelo, M., Mangiapan, S., Bagnati, R., Benfenati, E., and Fanelli, R.: Increased  
775 concentrations of nitrophenols in leaves from a damaged forestal site, *Chemosphere*,  
776 38, 1495-1503, [http://dx.doi.org/10.1016/S0045-6535\(98\)00370-1](http://dx.doi.org/10.1016/S0045-6535(98)00370-1), 1999.

777 Olariu, R. I., Klotz, B., Barnes, I., Becker, K. H., and Mocanu, R.: FT-IR study of the  
778 ring-retaining products from the reaction of OH radicals with phenol, o-, m-, and p-  
779 cresol, *Atmospheric Environment*, 36, 3685-3697,  
780 [http://dx.doi.org/10.1016/S1352-2310\(02\)00202-9](http://dx.doi.org/10.1016/S1352-2310(02)00202-9), 2002.

781 Pankow, J. F.: An absorption model of the gas/aerosol partitioning involved in the  
782 formation of secondary organic aerosol, *Atmospheric Environment*, 28, 189-193, Doi:  
783 10.1016/1352-2310(94)90094-9, 1994.

784 Platz, J., Nielsen, O. J., Wallington, T. J., Ball, J. C., Hurley, M. D., Straccia, A. M.,  
785 Schneider, W. F., and Sehested, J.: Atmospheric Chemistry of the Phenoxy Radical,  
786 C<sub>6</sub>H<sub>5</sub>O(•): UV Spectrum and Kinetics of Its Reaction with NO, NO<sub>2</sub>, and O<sub>2</sub>, *The*  
787 *Journal of Physical Chemistry A*, 102, 7964-7974, 10.1021/jp9822211, 1998.

788 Rippen, G., Zietz, E., Frank, R., Knacker, T., and Klöpffer, W.: Do airborne nitrophenols  
789 contribute to forest decline?, *Environmental Technology Letters*, 8, 475-482,  
790 10.1080/09593338709384508, 1987.

791 Rubio, M. A., Lissi, E., Herrera, N., Pérez, V., and Fuentes, N.: Phenol and nitrophenols  
792 in the air and dew waters of Santiago de Chile, *Chemosphere*, 86, 1035-1039,  
793 <http://dx.doi.org/10.1016/j.chemosphere.2011.11.046>, 2012.

794 Sander, R.: Compilation of Henry's law constants (version 4.0) for water as solvent,  
795 *Atmospheric Chemistry and Physics*, 15, 4399-4981, 10.5194/acp-15-4399-2015, 2015.

796 Schwarzenbach, R. P., Stierli, R., Folsom, B. R., and Zeyer, J.: Compound properties  
797 relevant for assessing the environmental partitioning of nitrophenols, *Environmental*  
798 *Science & Technology*, 22, 83-92, 10.1021/es00166a009, 1988.

799 Sekimoto, K., Inomata, S., Tanimoto, H., Fushimi, A., Fujitani, Y., Sato, K., and  
800 Yamada, H.: Characterization of nitromethane emission from automotive exhaust,  
801 *Atmospheric Environment*, 81, 523-531, 10.1016/j.atmosenv.2013.09.031, 2013.

802 Stark, H., Yatavelli, R. L. N., Kimmel, J. R., Bertram, T. H., Thornton, J. A., Jimenez, J.  
803 L., and Worsnop, D. R.: Cluster Formation and Ion Chemistry in the High Pressure  
804 Inlet of a Chemical Ionization Mass Spectrometer: Lessons learned from Field and  
805 Laboratory Studies, 22nd International Symposium on Gas Kinetics, June 18-22, 2012,  
806 Boulder, CO, 2012.

807 Stark, H., Yatavelli, R. L. N., Thompson, S. L., Kimmel, J. R., Cubison, M. J., Chhabra,  
808 P. S., Canagaratna, M. R., Jayne, J. T., Worsnop, D. R., and Jimenez, J. L.: Methods to  
809 extract molecular and bulk chemical information from series of complex mass spectra  
810 with limited mass resolution, *International Journal of Mass Spectrometry*,  
811 10.1016/j.ijms.2015.08.011, 2015.

812 Stockwell, C. E., Veres, P. R., Williams, J., and Yokelson, R. J.: Characterization of  
813 biomass burning emissions from cooking fires, peat, crop residue, and other fuels with  
814 high-resolution proton-transfer-reaction time-of-flight mass spectrometry, *Atmos.*  
815 *Chem. Phys.*, 15, 845-865, 10.5194/acp-15-845-2015, 2015.

816 Tremp, J., Mattle, P., Fingler, S., and Giger, W.: Phenols and nitrophenols as  
817 tropospheric pollutants: Emissions from automobile exhausts and phase transfer in the  
818 atmosphere, *Water Air Soil Pollut*, 68, 113-123, 10.1007/BF00479396, 1993.

819 Veres, P., Roberts, J. M., Warneke, C., Welsh-Bon, D., Zahniser, M., Herndon, S., Fall,  
820 R., and de Gouw, J.: Development of negative-ion proton-transfer chemical-ionization  
821 mass spectrometry (NI-PT-CIMS) for the measurement of gas-phase organic acids in  
822 the atmosphere, *International Journal of Mass Spectrometry*, 274, 48-55, DOI  
823 10.1016/j.ijms.2008.04.032, 2008.

824 Vione, D., Maurino, V., Minero, C., and Pelizzetti, E.: Phenol photolysis upon UV  
825 irradiation of nitrite in aqueous solution I: Effects of oxygen and 2-propanol,  
826 *Chemosphere*, 45, 893-902, [http://dx.doi.org/10.1016/S0045-6535\(01\)00035-2](http://dx.doi.org/10.1016/S0045-6535(01)00035-2),  
827 2001.

828 Vione, D., Maurino, V., Minero, C., and Pelizzetti, E.: Aqueous Atmospheric Chemistry:  
829 Formation of 2,4-Dinitrophenol upon Nitration of 2-Nitrophenol and 4-Nitrophenol in  
830 Solution, *Environmental Science & Technology*, 39, 7921-7931, 10.1021/es050824m,  
831 2005.

832 Vione, D., Maurino, V., Minero, C., Duncianu, M., Olariu, R.-I., Arsene, C., Sarakha, M.,  
833 and Mailhot, G.: Assessing the transformation kinetics of 2- and 4-nitrophenol in the  
834 atmospheric aqueous phase. Implications for the distribution of both nitroisomers in the  
835 atmosphere, *Atmospheric Environment*, 43, 2321-2327,  
836 <http://dx.doi.org/10.1016/j.atmosenv.2009.01.025>, 2009.

837 Warneke, C., Geiger, F., Edwards, P. M., Dube, W., Pétron, G., Kofler, J., Zahn, A.,  
838 Brown, S. S., Graus, M., Gilman, J., Lerner, B., Peischl, J., Ryerson, T. B., de Gouw, J.  
839 A., and Roberts, J. M.: Volatile organic compound emissions from the oil and natural  
840 gas industry in the Uinta Basin, Utah: point sources compared to ambient air  
841 composition, *Atmos. Chem. Phys.*, 14, 10977-10988, 10.5194/acpd-14-11895-2014,  
842 2014.

843 Warneke, C., Veres, P. R., Murphy, S. M., Soltis, J., Field, R. A., Graus, M. G., Koss, A.,  
844 Li, S. M., Li, R., Yuan, B., Roberts, J. M., and de Gouw, J. A.: PTR-QMS vs. PTR-  
845 TOF comparison in a region with oil and natural gas extraction industry in the Uintah  
846 Basin in 2013, *Atmos. Meas. Tech.*, 8, 411-420, 10.5194/amtd-7-6565-2014, 2015.

847 Wild, R. J., Edwards, P. M., Dube, W. P., Baumann, K., Edgerton, E. S., Quinn, P. K.,  
848 Roberts, J. M., Rollins, A. W., Veres, P. R., Warneke, C., Williams, E. J., Yuan, B.,  
849 and Brown, S. S.: A Measurement of Total Reactive Nitrogen, NO<sub>y</sub>, together with  
850 NO<sub>2</sub>, NO, and O<sub>3</sub> via Cavity Ring-down Spectroscopy, *Environ Sci Technol*, 48,  
851 9609-9615, 10.1021/es501896w, 2014.

852 Yatavelli, R. L. N., Stark, H., Thompson, S. L., Kimmel, J. R., Cubison, M. J., Day, D.  
853 A., Campuzano-Jost, P., Palm, B. B., Hodzic, A., Thornton, J. A., Jayne, J. T.,  
854 Worsnop, D. R., and Jimenez, J. L.: Semicontinuous measurements of gas-particle  
855 partitioning of organic acids in a ponderosa pine forest using a MOVI-HRToF-CIMS,  
856 *Atmos. Chem. Phys.*, 14, 1527-1546, 10.5194/acp-14-1527-2014, 2014.

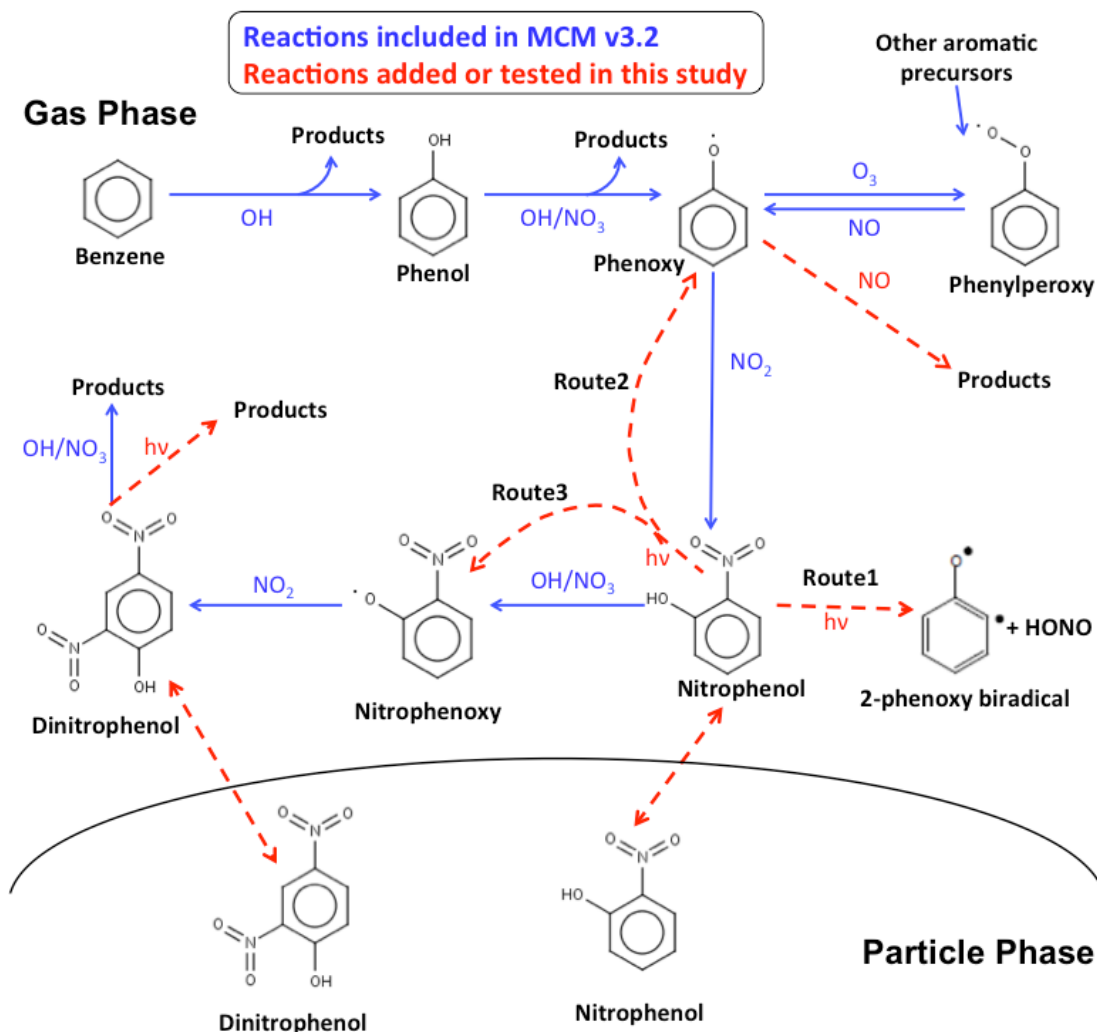
857 Yuan, B., Veres, P. R., Warneke, C., Roberts, J. M., Gilman, J. B., Koss, A., Edwards, P.  
858 M., Graus, M., Kuster, W. C., Li, S. M., Wild, R. J., Brown, S. S., Dubé, W. P., Lerner,  
859 B. M., Williams, E. J., Johnson, J. E., Quinn, P. K., Bates, T. S., Lefer, B., Hayes, P. L.,  
860 Jimenez, J. L., Weber, R. J., Zamora, R., Ervens, B., Millet, D. B., Rappenglück, B.,  
861 and de Gouw, J. A.: Investigation of secondary formation of formic acid: urban  
862 environment vs. oil and gas producing region, *Atmos. Chem. Phys.*, 15, 1975-1993,  
863 10.5194/acp-15-1975-2015, 2015.

864 Zhang, X., Lin, Y.-H., Surratt, J. D., and Weber, R. J.: Sources, Composition and  
865 Absorption Ångström Exponent of Light-absorbing Organic Components in Aerosol  
866 Extracts from the Los Angeles Basin, *Environmental Science & Technology*, 47, 3685-  
867 3693, 10.1021/es305047b, 2013.

868

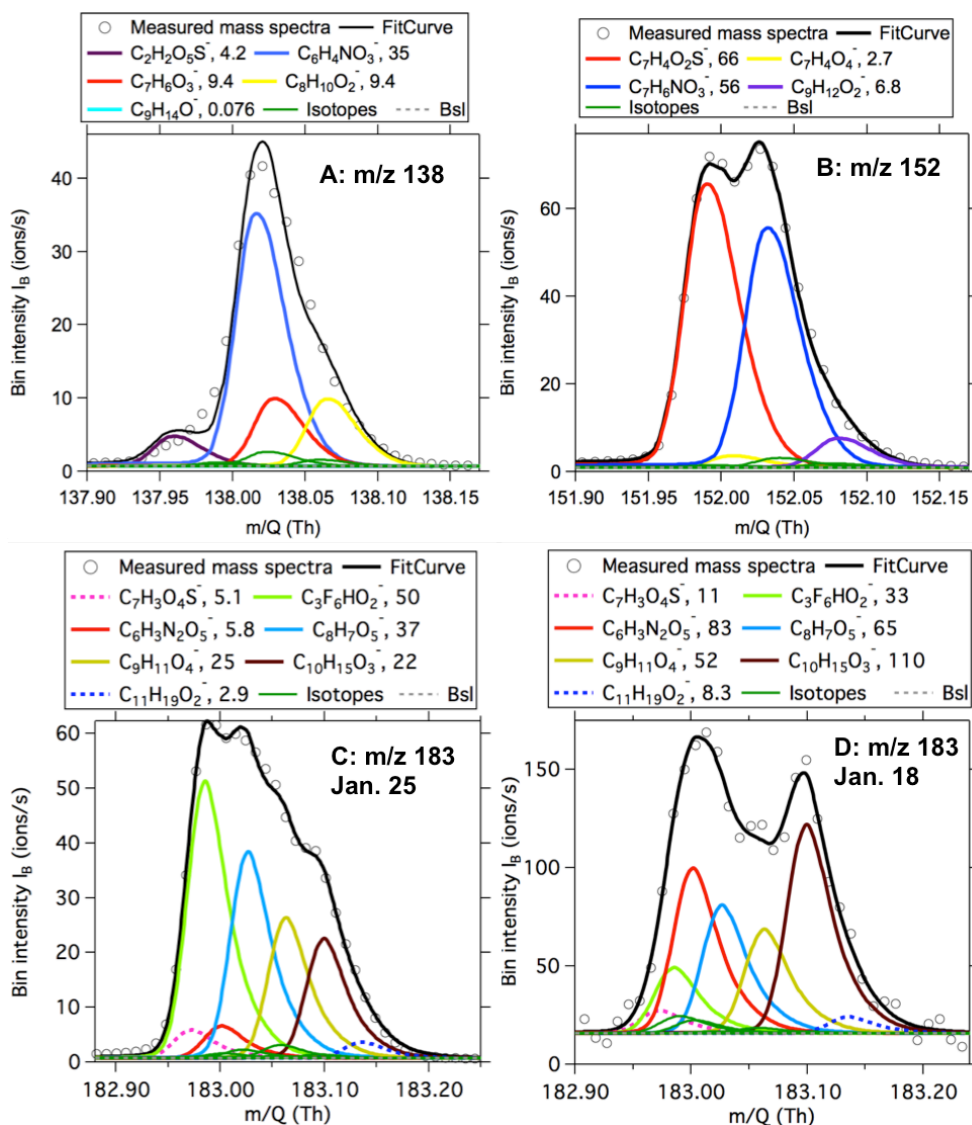
869

870 **Figures**



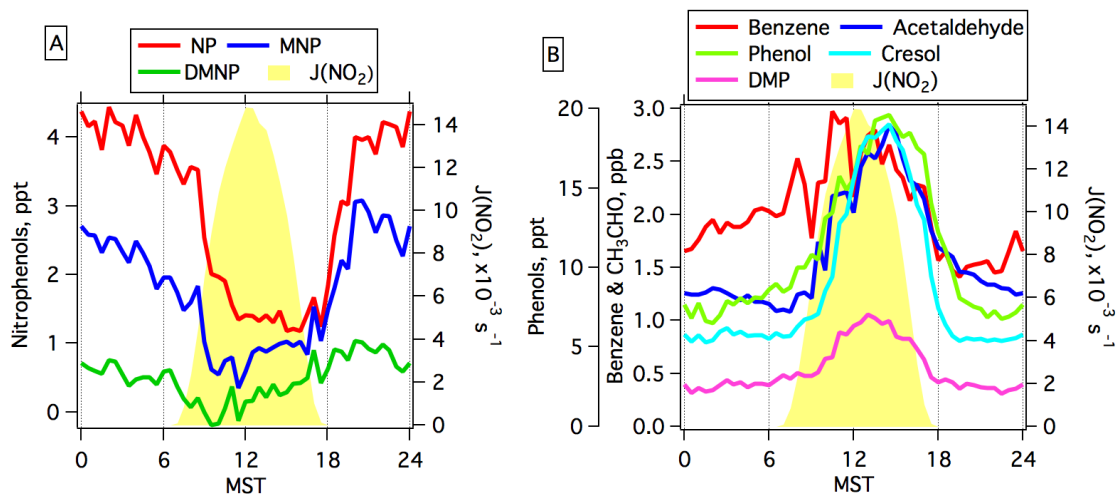
871  
872  
873  
874  
875  
876  
877  
878

Figure 1. Formation of phenol, nitrophenol (NP) and dinitrophenol (DNP) from the photo-oxidation of benzene in the atmosphere (Jenkin et al., 2003). Reactions in blue are included in the MCM v3.2, whereas reactions in red are added or evaluated in this study. For NP, DNP and the intermediate radicals, other isomers are expected but not shown for the sake of clarity.



879  
 880  
 881  
 882  
 883  
 884

Figure 2. High-resolution peak fitting to the averaged mass spectra of acetate ToF-CIMS for  $m/z$  138 (A),  $m/z$  152 (B) and  $m/z$  183 (C) on January 25, 2014 and  $m/z$  183 (D) on Jan. 18, 2014 during UBWOS 2014. The dark green lines indicate the calculated isotope signals from lower masses.



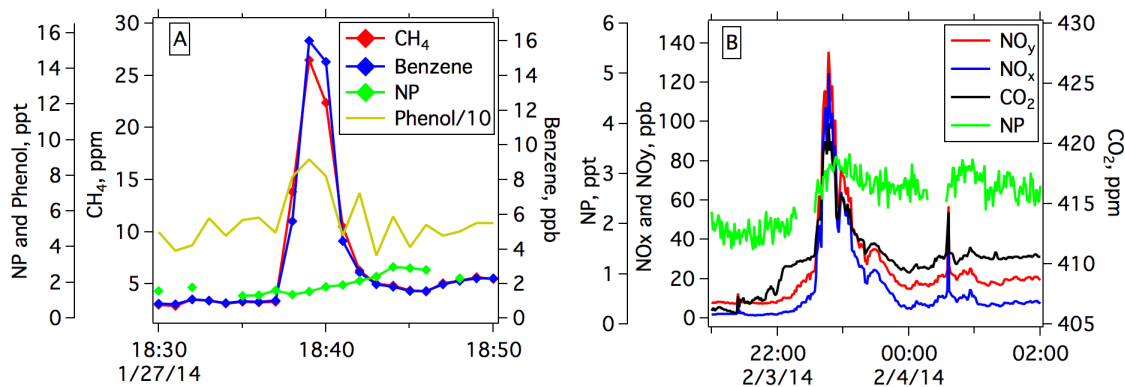
885

886 Figure 3. (A) Diurnal profiles of measured NP, MNP, DMNP. (B) Diurnal profiles of

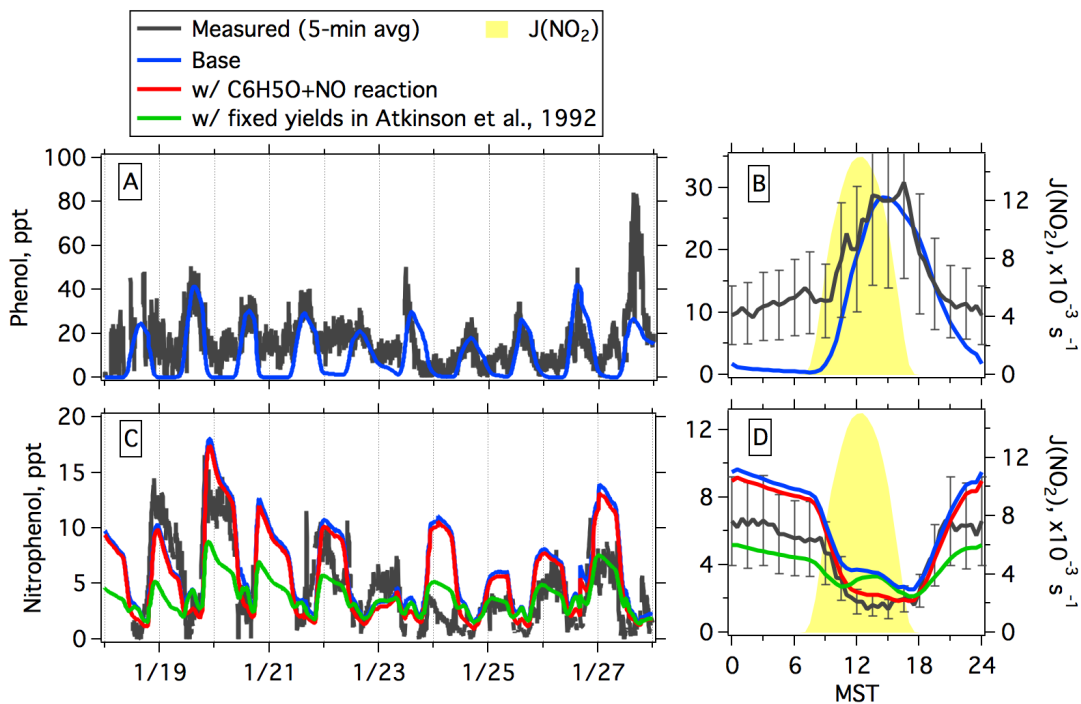
887 benzene, acetaldehyde, phenol, cresol and DMP. Photolysis frequencies of NO<sub>2</sub> are

888 shown in both A and B for reference.

889

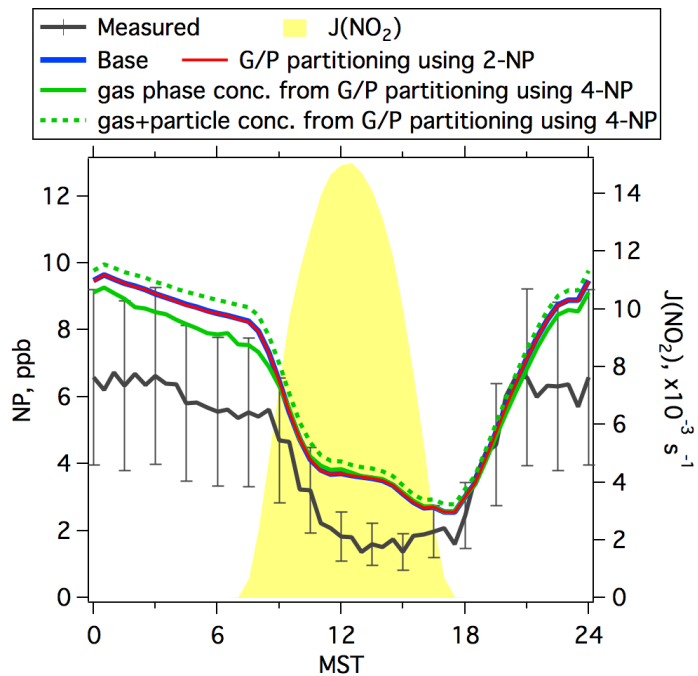


890  
 891 Figure 4. (A) An episode with high concentrations of methane and benzene on January  
 892 27, 2014 during UBWOS 2014. The source for this episode was fugitive emissions from  
 893 oil and gas activities. (B) An episode with high concentrations of NO<sub>y</sub> and CO<sub>2</sub> on  
 894 February 3, 2014 during UBWOS 2014. The source for this episode was fuel combustion  
 895 (e.g., vehicle exhaust and/or other combustion sources for oil and gas extraction).

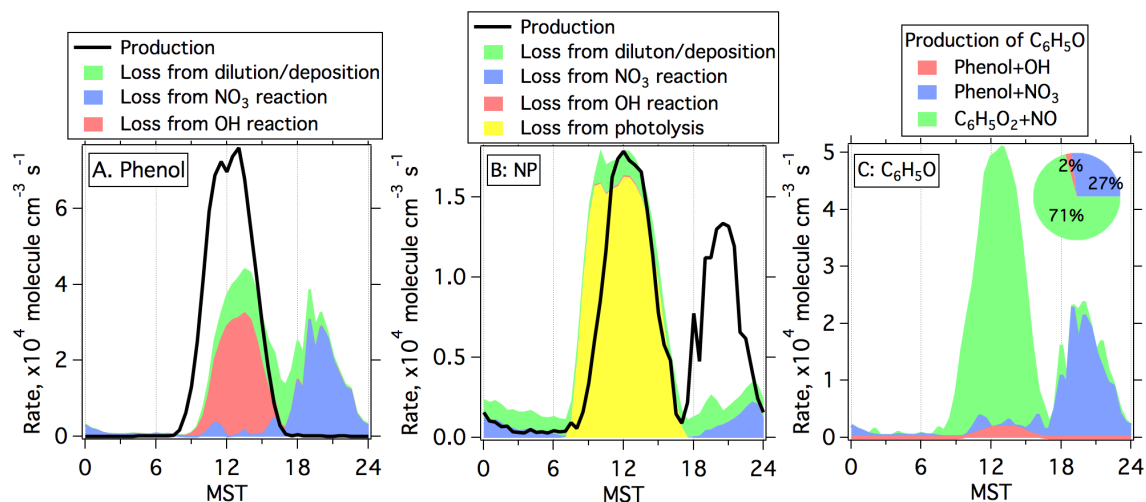


896  
 897  
 898  
 899  
 900  
 901  
 902

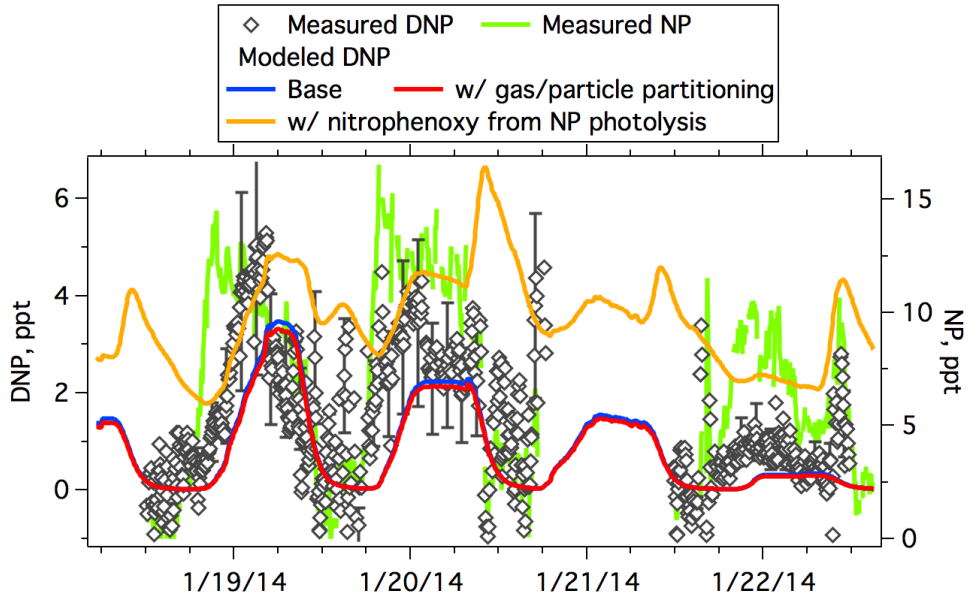
Figure 5. (A and C) Comparison of measured and modeled time series of phenol (A) and NP (C). (B and D) Diurnal profiles of measured and modeled concentrations of phenol (B) and NP (D). Photolysis frequencies of NO<sub>2</sub> are shown in B and D for reference. Error bars in (B) and (D) indicate the accuracies of measured concentrations of phenol (50%) and NP (40%), respectively.



903  
 904 Figure 6. Diurnal profiles of measured and modeled concentrations of NP from the base  
 905 simulation and the simulations considering gas/particle partitioning. Photolysis  
 906 frequencies of NO<sub>2</sub> are shown for reference. Error bars indicate the accuracies of  
 907 measured concentrations of NP (40%).  
 908

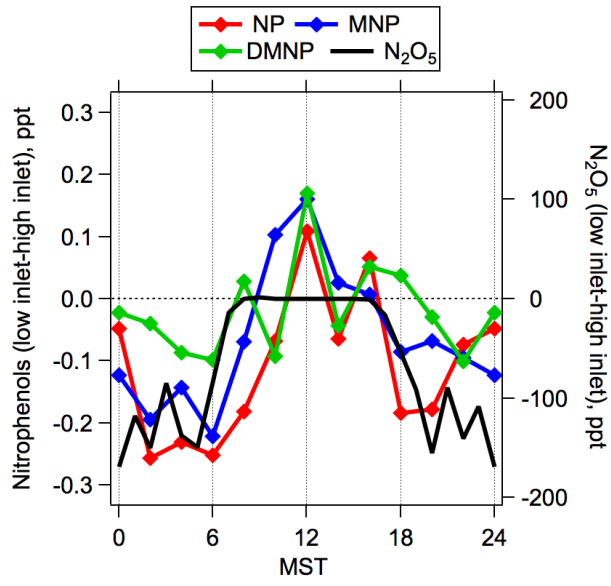


909  
 910 Figure 7. Diurnal profiles of production and loss rates from different pathways for phenol  
 911 (A) and NP (B) derived from the base simulation of the box model. (C) Diurnal profiles  
 912 of production rates from different pathways for  $\text{C}_6\text{H}_5\text{O}$  radicals. The inserted pie in C  
 913 shows contributions from three different pathways to formation of  $\text{C}_6\text{H}_5\text{O}$  radicals on a  
 914 daily basis.  
 915



916  
 917 Figure 8. Comparison of measured and modeled time series of DNP. Measured time  
 918 series of NP is also shown for comparison. Error bars indicate the accuracies of measured  
 919 DNP concentrations (50%).

920  
 921



922  
 923 Figure 9. Diurnal profiles of vertical gradients for nitrated phenols measured in January  
 924 22 – February 1. The measured vertical gradient of N<sub>2</sub>O<sub>5</sub> measured in February 6- 14 is  
 925 also shown for comparison.  
 926

927 **Tables**

928 Table 1. Sensitivities and detection limits of nitrated phenols in acetate ToF-CIMS

Species	Abbreviation	Ion	$m/z$	Sensitivity		Detection Limit, ppt <sup>f</sup>	
				Value, ncps/ppt	Ratio to HCOOH <sup>e</sup>	Method 1	Method 2
Nitrophenol	NP	C <sub>6</sub> H <sub>4</sub> NO <sub>3</sub> <sup>-</sup>	138.0197	13.2 <sup>a</sup>	2.6	0.18	0.45
Methylnitrophenol	MNP	C <sub>7</sub> H <sub>6</sub> NO <sub>3</sub> <sup>-</sup>	152.0353	16.6 <sup>b</sup>	3.3	0.24	0.36
Dimethylnitrophenol + ethylnitrophenol	DMNP	C <sub>8</sub> H <sub>8</sub> NO <sub>3</sub> <sup>-</sup>	166.0510	16.6 <sup>c</sup>	3.3	0.14	0.36
Dinitrophenol	DNP	C <sub>6</sub> H <sub>3</sub> N <sub>2</sub> O <sub>5</sub> <sup>-</sup>	183.0047	10.3 <sup>d</sup>	2.0	0.23	0.58

929 a: Average from calibrations of 2-NP (8.4 ncps/ppt) and 4-NP (18.0 ncps/ppt).

930 b: Calibration of 2-methyl-4-nitrophenol.

931 c: Using the same value as MNP.

932 d: Calibration using 2,5-dinitrophenol.

933 e: Based on the determined sensitivity of formic acid (HCOOH) at 5.0 ncps/ppt during UBWOS  
934 2014.935 f: Method 1 is based on the random errors of observed counts follow Poisson distribution,  
936 whereas method 2 is calculated as the concentrations with counts at three times of standard  
937 deviations of measured background counts (see discussions in text and in Bertram et al. (2011)).

938

939

940

941

942

943

944 Table 2. Vapor pressure, enthalpy of evaporation ( $\Delta H_{vap}$ ) and calculated concentration  
945 fractions in particle phase ( $F_p$ ) for several nitrated phenols

Species	Vapor pressure at 298 K, Torr <sup>a</sup>	$\Delta H_{vap}$ , kJ/mol <sup>a</sup>	$F_p$ ,
2-NP	0.20	53.1	$1.1 \pm 0.9 \times 10^{-4}$
4-NP	$1.4 \times 10^{-3}$	80.0	$5.3 \pm 4.8 \times 10^{-2}$
2,4-DNP	$8.4 \times 10^{-3}$	70.4	$4.6 \pm 4.4 \times 10^{-3}$
2,5-DNP	$1.2 \times 10^{-3}$	68.5	$2.8 \pm 2.7 \times 10^{-3}$

946 a: Calculated from data in Schwarzenbach et al. (1988).